GLIA

WILEY

RESEARCH ARTICLE

Loss of glutamate transporter *eaat2a* leads to aberrant neuronal excitability, recurrent epileptic seizures, and basal hypoactivity

Adriana L. Hotz[1,2] [ID] | Ahmed Jamali[3] | Nicolas N. Rieser[1,2] [ID] |
Stephanie Niklaus[1] [ID] | Ecem Aydin[3] | Sverre Myren-Svelstad[3,4,5] [ID] |
Laetitia Lalla[3] | Nathalie Jurisch-Yaksi[3,4,6] [ID] | Emre Yaksi[3] [ID] |
Stephan C. F. Neuhauss[1] [ID]

[1]Department of Molecular Life Sciences, University of Zurich, Zurich, Switzerland

[2]Life Science Zürich Graduate School - Neuroscience, University of Zurich and ETH Zurich, Zurich, Switzerland

[3]Kavli Institute for Systems Neuroscience and Centre for Neural Computation, Faculty of Medicine and Health Sciences, Norwegian University of Science and Technology, Trondheim, Norway

[4]Department of Neurology and Clinical Neurophysiology, St. Olav's University Hospital, Trondheim, Norway

[5]Department of Neuromedicine and Movement Science, Faculty of Medicine and Health Sciences, Norwegian University of Science and Technology, Trondheim, Norway

[6]Department of Clinical and Molecular Medicine, Faculty of Medicine and Health Sciences, Norwegian University of Science and Technology, Trondheim, Norway

Correspondence
Stephan C. F. Neuhauss, Department of Molecular Life Sciences, University of Zurich, Winterthurerstrasse 190, 8057 Zurich, Switzerland.
Email: stephan.neuhauss@mls.uzh.ch

Nathalie Jurisch-Yaksi, Department of Clinical and Molecular Medicine, Faculty of Medicine and Health Sciences, Norwegian University of Science and Technology, Erling Skjalgsons Gate 1, 7491 Trondheim, Norway
Email: nathalie.jurisch-yaksi@ntnu.no

Emre Yaksi, Kavli Institute for Systems Neuroscience and Centre for Neural Computation, Faculty of Medicine and Health Sciences, Norwegian University of Science and Technology, Olav Kyrres gate 9, 7030 Trondheim, Norway
Email: emre.yaksi@ntnu.no

Present address
Stephanie Niklaus, EraCal Therapeutics, Schlieren, Switzerland

Abstract

Astroglial excitatory amino acid transporter 2 (EAAT2, GLT-1, and SLC1A2) regulates the duration and extent of neuronal excitation by removing glutamate from the synaptic cleft. Hence, an impairment in EAAT2 function could lead to an imbalanced brain network excitability. Here, we investigated the functional alterations of neuronal and astroglial networks associated with the loss of function in the astroglia predominant *eaat2a* gene in zebrafish. We observed that *eaat2a*$^{-/-}$ mutant zebrafish larvae display recurrent spontaneous and light-induced seizures in neurons and astroglia, which coincide with an abrupt increase in extracellular glutamate levels. In stark contrast to this hyperexcitability, basal neuronal and astroglial activity was surprisingly reduced in *eaat2a*$^{-/-}$ mutant animals, which manifested in decreased overall locomotion. Our results reveal an essential and mechanistic contribution of EAAT2a in balancing brain excitability, and its direct link to epileptic seizures.

KEYWORDS
astroglia, brain excitability, calcium imaging, eaat2, epilepsy, glutamate, zebrafish

1 | INTRODUCTION

Astroglia are the most numerous glial cells within the central nervous system (CNS). They do not only provide trophic support to neurons but also play an important role in synapse formation and neurotransmission (Allen & Eroglu, 2017; Bazargani & Attwell, 2016; Clarke & Barres, 2013; Santello et al., 2019). By taking up neurotransmitters from the synaptic cleft, these glial cells are crucial for regulating synaptic transmission. The excitatory amino acid transporter 2 (EAAT2), expressed mainly on astroglia, plays a key role in synaptic regulation by removing the majority of extracellular glutamate, which is the main excitatory neurotransmitter in the CNS (Coulter & Eid, 2012; Danbolt, 2001). Impaired glutamate clearance by this transporter has been shown to lead to synaptic accumulation of the neurotransmitter, resulting in an overactive CNS and excitotoxicity (Rothstein et al., 1996; Vandenberg & Ryan, 2013a). This in turn may cause epilepsy, a group of brain disorders characterized by recurrent seizures (Fisher et al., 2014).

Previous studies have shown that astroglia-neuron interactions may play an essential role in seizure initiation and propagation (Devinsky, Vezzani, Najjar, Lanerolle, & Rogawski, 2013; Diaz Verdugo et al., 2019; Steinhäuser et al., 2012). On one hand, the functional coupling of astroglia through gap junctions is crucial to avert excessive neuronal activation, accomplished by rapid redistribution of ions and neurotransmitters across the connected astroglial network (Steinhäuser et al., 2012). On the other hand, this functional syncytium might also, under special circumstances, promote epileptogenesis (Rosch & Dulla, 2020). The intercellular spread of calcium waves among astroglia can affect neuronal synchronization and therefore influence the propagation of seizure activity (Diaz Verdugo et al., 2019). In addition, disruptions of the glutamate-glutamine cycle, in which EAAT2 is essential, are linked with temporal lobe epilepsy in human patients and rodents (Coulter & Steinhäuser, 2015; Eid et al., 2019). Accordingly, it is essential to understand how loss of EAAT2 affects neurons and astroglia.

In the present study, we generated a zebrafish (*Danio rerio*) mutant lacking EAAT2a, the zebrafish orthologue matching the mammalian EAAT2 in biophysical characteristics and mainly glial expression pattern (Gesemann et al., 2010; Niklaus et al., 2017). Calcium imaging in the transparent zebrafish larvae allowed us to image whole-brain network activity in vivo (Vladimirov et al., 2014). We show that loss of EAAT2a transporter in larval zebrafish leads to increased brain excitability and recurrent spontaneous seizures, mimicking a human phenotype of patients with de novo mutations in EAAT2 (Epi4K Consortium, 2016; Guella et al., 2017). These seizures are manifested in zebrafish larvae by epileptic locomotor bursts and periods of excessive brain activity, accompanied by massively increased extracellular glutamate concentrations. Counterintuitively, between these periods of hyperexcitation, neuronal and astroglial network activity of $eaat2a^{-/-}$ mutants is reduced. This coincides with a decreased overall locomotion compared to their unaffected siblings, and mirrors slow background brain activity and reduced muscle tone present in human patients (Epi4K Consortium et al., 2013; Epi4K Consortium, 2016; Guella et al., 2017). Altogether, our in vivo model of impaired EAAT2a function results in a depressed yet hyperexcitable brain state, and mimics a form of developmental and epileptic encephalopathy (DEE).

2 | MATERIAL AND METHODS

2.1 | Fish husbandry and handling

Zebrafish (*Danio rerio*) were kept under standard conditions (Mullins et al., 1994). In this study, WIK and Tübingen wild-type strains were used. For calcium or glutamate imaging experiments, $eaat2a^{+/-}$ mutant animals were outcrossed with $Tg(elavl3:GCaMP5G);nacre^{-/-}$ (Akerboom et al., 2012) (epifluorescence microscope), $Tg(gfap:Gal4)$ $nw7;Tg(UAS:GCaMP6s)$ (Diaz Verdugo et al., 2019; Muto et al., 2017) (two-photon spontaneous recordings), $Tg(elavl3:GCaMP6s)$ (Vladimirov et al., 2014) (two-photon light-stimulation recordings) and $Tg(gfap:iGluSnFR)$ (MacDonald et al., 2016) fish. For experiments, adult $eaat2a^{+/-}$ animals were set up pairwise and embryos were raised in E3 medium (5 mM NaCl, 0.17 mM KCl, 0.33 mM CaCl2, 0.33 mM MgSO4, 10^{-5}% methylene blue) (Zürich) or in egg water (60 mg/L marine salt, 10^{-4}% methylene blue) (Trondheim) at 28°C with 10:14 h dark:light cycle. As control, $eaat2a^{-/-}$ larvae were compared to $eaat2a^{+/+}$ and $eaat2a^{+/-}$ siblings. In all imaging experiments where the larva was immobilized, the cerebral blood flow was assessed in the prosencephalic arteries or anterior cerebral veins (Isogai et al., 2001) before and after the experiment, and animals without cerebral blood flow were excluded from the final analysis. All experiments were conducted in accordance with local authorities (Zürich Switzerland: Kantonales Veterinäramt TV4206, Trondheim Norway: directive 2010/63/EU of the European Parliament and the Council of the European Union and the Norwegian Food Safety Authorities).

2.2 | In situ hybridization

eaat2a (ENSDARG00000102453) cloning into the TOPO pCRII vector (TA Cloning Kit Dual Promoter, Invitrogen, Basel, Switzerland) and preparation of digoxigenin (DIG)-labeled antisense RNA probes is described elsewhere (Gesemann et al., 2010; Niklaus et al., 2017). RNA probes were applied on whole-mount zebrafish larvae (3 and 5 days post fertilization [dpf]) and adult (older than 6 months) brain cross sections at a concentration of 2 ng/μl at 64°C overnight (Huang

et al., 2012). For larval brain sections, representative stained and para-formaldehyde (PFA) post-fixed embryos were cryoprotected in 30% sucrose at 4°C overnight, embedded in Tissue Freezing Medium TFMTM (Electron Microscopy Sciences), cryo-sectioned at 14–16 μm and mounted onto Superfrost slides (Thermo Fisher Scientific). PFA post-fixed whole-mount embryos (in glycerol) and sections were imaged with an Olympus BX61 brightfield microscope. Images were adjusted for brightness and contrast using Affinity Photo Version 1.8 and assembled in Affinity Designer Version 1.7.

2.3 | Immunohistochemistry

Generation of the chicken anti-EAAT2a (zebrafish) antibody is described elsewhere (Niklaus et al., 2017). Five dpf larvae were fixed in 4% PFA in phosphate buffered saline (PBS, pH 7.4) at room temperature for 40 min. Embryos were cryo-protected in 30% sucrose in PBS at 4°C overnight, embedded in Tissue Freezing Medium TFMTM (Electron Microscopy Sciences), cryo-sectioned at 14–16 μm and mounted onto Superfrost slides (Thermo Fisher Scientific). Immuno-histochemistry was performed as described before (Niklaus et al., 2017). Chicken anti-EAAT2a 1:500, mouse anti-synaptic vesicle 2 (IgG1, 1:100, DSHB USA), mouse anti-acetylated tubulin (IgG2b, 1:500, Sigma 7451) and mouse anti–glutamine synthetase (IgG2a, 1:200, EMD Millipore, MAB302) were used as primary antibodies. Secondary antibodies were goat anti-chicken Alexa Fluor 488, goat anti-mouse IgG2a Alexa Fluor 568, goat anti-mouse IgG2b Alexa Fluor 647 and goat anti-mouse IgG1 Alexa Fluor 647, all 1:500 (all from Invitrogen, Thermo Fisher Scientific). Slides were cover-slipped using Mowiol (Polysciences) containing DABCO (Sigma-Aldrich) and imaged with a TCS LSI confocal microscope (Leica Microsystems). Images were adjusted for brightness and contrast using Affinity Photo Version 1.8 and assembled in Affinity Designer Version 1.7.

2.4 | CRISPR/Cas9-mediated mutagenesis and genotyping

CRISPR target sites for *eaat2a* (ENSDARG00000102453) of the 5′-GG (N18)NGG-3′ motif favorable for T7-mediated in vitro transcription (Gagnon et al., 2014) were selected using the https://chopchop.cbu.uib. no/ and www.zifit.partners.org prediction tools. Synthesis of single guide RNA (sgRNA) was performed using a PCR based approach as follows. dsDNA of the target region was amplified with a high fidelity Phusion polymerase (New England Bio Labs) using the forward primer sg1 together with the common reverse primer sg2 (Supplementary Table 1). sgRNA was T7 in vitro transcribed (MEGAshortscriptTM T7 Transcription Kit, Ambion) and subsequently purified using the MEGAclearTM Kit (Ambion).

The injection mix consisting of 160 ng/μl sgRNA, 1 μg/μl Cas 9 protein (Flag/ or GFP-tagged Cas9 kindly provided by Prof. Dr. C. Mosimann and Prof. Dr. M. Jineck) and 300 mM KCl was incubated at 37°C for 10 min to enable Cas9/sgRNA complex formation. One-cell staged embryos were injected with 1 nl injection mix into the cell. Mutation rate

efficiency was tested by genotyping a pool of around 10–15 injected F0 larvae per clutch while their siblings were raised to adulthood. Adult F0 crispant fish were outcrossed to Tübingen wild-type animals. F1 embryos were genotyped at 3 dpf by larval tail biopsies (Wilkinson, Elworthy, Ingham, & van Eeden, Fredericus J M, 2013) and raised in single tanks. The *eaat2a* target site was PCR amplified with a fast-cycling polymerase (KAPA2G Fast HotStart PCR kit, KAPA Biosystems) (primers: sense (fw) and antisense (rev), Supplementary Table 1). Amplicons were cloned into pCR 2.1-TOPO vectors (Invitrogen) and sequenced. The resulting heterozygous mutant line carrying one copy of a − 13 null allele was repeatedly outcrossed to wild-type and transgenic fish to generate stable heterozygous F2, F3, and F4 generations.

eaat2a mutant fish can be genotyped by the above-mentioned PCR amplification and a subsequent gel-electrophoresis, which allows detection of the 13 base pair deletion. Larvae were genotyped after each experiment. After two-photon microscopy, all larvae were genotyped by means of a PCR melting curve analysis using SYBR Green (PowerUp SYBR Green Master Mix, Thermo Fisher Scientific). For RT-qPCR experiments, wild-type progeny of $eaat2a^{+/-}$ incrosses were selected by pregenotyping using the Zebrafish Embryo Genotyper (ZEG, wFluidx) as described previously (Lambert et al., 2018). Briefly, 3–4 dpf embryos were loaded individually onto the ZEG chip in 12 μl E3 and vibrated for 10 min at 1.4 Volts. Subsequently, 8 μl of each sample E3 was used directly for PCR as described above (KAPA Biosystems). Embryos were kept in 48-well plates until genotyping was achieved.

2.5 | Zebrafish survival analysis and length measurements

Embryos were raised separately in 24-well plates containing 1.5 ml E3 medium, which was changed daily. From 5 dpf on, larvae were fed manually. Animal survival was monitored daily over an 11-day period. From 1 to 7 dpf, larvae were temporarily anesthetized by tricaine (0.2 mg/ml) and individually imaged with an Olympus MVX10 microscope. Body lengths were measured along the spinal cord using Fiji ImageJ (Schindelin et al., 2012) and further analyzed using R software version 3.6.0 with the RStudio version 1.2.1335 interface (R Core Team, 2019; RStudio Team, 2018).

2.6 | Behavioral analysis

Swimming patterns of 5 dpf larvae were recorded using the ZebraBox system (ViewPoint Life Sciences). The room was kept at 27°C throughout the recordings. Larvae were individually placed at randomized positions of 48-well plates containing 1 ml E3 medium and transferred into the recording chamber for a minimum of 10 min acclimatization. Subsequently, recordings of 30 min in normal light conditions (20% light intensity) were performed. An automated camera tracked individual larvae (threshold black 30) and detected the distance and duration moved by each larva exceeding 1 mm per second in accumulating five-second intervals. Data processing and analysis was done with a custom code written in R with the RStudio interface (R Core Team, 2019; RStudio Team, 2018).

Software-related artifacts were removed in a blinded manner. Velocity of long-lasting bursts were calculated as distance divided by time for every five-second interval in which the animal moved at least 3.5 s.

2.7 | Combined LFP experiments together with epifluorescence iGluSnFR imaging

Simultaneous local field potential (LFP) recordings of seizure activity and epifluorescence imaging of iGluSnFR signals were performed in 5 dpf Tg(gfap:iGluSnFR) zebrafish larvae (Diaz Verdugo et al., 2019). First, zebrafish larvae were paralyzed by α-bungarotoxin injection (Reiten et al., 2017). Next, the larvae were embedded in 1%–1.5% low melting point agarose (Fisher Scientific) in a recording chamber (Fluorodish, World Precision Instruments) and kept in artificial fish water (AFW, 1.2 g marine salt in 20 L RO water). For exposure with pentylenetetrazole (PTZ), AFW was replaced by 20 mM PTZ (in AFW) after placing the LFP electrode. For LFP recordings, a borosilicate glass patch clamp pipette (9–15 MOhms) loaded with teleost artificial cerebrospinal fluid (Mathieson & Maler, 1988) (ACSF, containing in mM: 123.9 NaCl, 22 D-glucose, 2 KCl, 1.6 MgSO$_4$ · 7H$_2$O, 1.3 KH$_2$PO$_4$, 24 NaHCO$_3$, 2 CaCl$_2$ 2H$_2$O) was inserted in the forebrain (Zhang et al., 2015). LFP recordings were performed by a MultiClamp 700B amplifier, in current clamp mode at 10 kHz sampling rate, and band pass filtered at 0.1–1000 Hz. For imaging iGluSnFR signals, microscopy images were collected at 1 Hz sampling rate, using a Teledyne QImaging QI825 camera, in combination with Olympus BX51 fluorescence microscope and Olympus UMPLANFL 40X water immersion objective. Data acquisition of LFP signals were done in MATLAB (Mathworks), and iGluSnFR signals were done in Ocular Image Acquisition Software.

All data were analyzed using MATLAB (Mathworks). LFP voltage traces were down sampled from 10 kHz to 1 Hz ('resample' function with 'pchip' method, MATLAB). Mean iGluSnFR fluorescence signal was extracted for each frame. Change in fluorescence (ΔF/F$_0$) relative to baseline (F$_0$) was computed with F$_0$ as the 8% of a moving window of 80 s, which was then smoothed with the same time window using a linear interpolation with a step size of 1 s (Romano et al., 2017). Seizure-like events were detected from ΔF/F$_0$ ('findpeaks' function, MATLAB) with a minimum peak height, and prominence, of 5%. The median of half-height width of the curves was used to calculate median duration.

2.8 | Quantitative reverse transcription PCR

Preselected 5 dpf larvae were anesthetized on ice and brains dissected using an insect pin and a syringe needle in a dish containing RNA later (Sigma-Aldrich). To confirm genotype, remaining tissue was lysed and gDNA amplified by means of PCR (KAPA Biosystems) as described above. Total RNA of equal pools of larval brains was extracted using the ReliaPrep kit (Promega). RNA was reverse transcribed to cDNA using the Super Script III First-strand synthesis system (Invitrogen) using 1:1 ratio of random hexamers and oligo (dt) primers.

The qPCR reactions were performed using SsoAdvanced Universal SYBR Green Supermix on a CFX96 Touch Real-Time PCR

Detection System (Bio-rad). Primer (Supplementary Table 2) efficiencies were calculated by carrying out a dilution series. After the primer efficiencies were determined equal, brain samples were used for qPCR using 10 ng of cDNA per reaction. The controls "no reverse transcription control" (nRT control) and "no template control" (NTC) were performed with every qPCR reaction. g6pd and b2m were chosen as reference genes. All reactions were performed in technical triplicates. Data was analyzed in CFX Maestro Software from Bio-Rad and Microsoft Excel. Statistical analysis was performed between dCt values.

2.9 | Calcium imaging and data analysis

2.9.1 | Epifluorescence microscope

Five dpf larvae in the Tg(elavl3:GCaMP5G) background were individually immobilized in a drop of 1.8% NuSieveTM GTGTM low melting temperature agarose (Lonza) with the tail freed from agarose in a small cell culture dish (Corning Incorporated) filled with water. Calcium signals were recorded using an Olympus BX51 WI epifluorescence microscope and by means of a camera (4 Hz sampling rate) with a 20× water immersion objective and the VisiView software established by the Visitron Systems GmbH.

In each experiment, the GCaMP5G fluorescence signal of manually selected ROIs (whole brain, anterior forebrain, midbrain, and hindbrain) was extracted using Fiji ImageJ (Schindelin et al., 2012). For each time point, the mean intensity of each ROI was measured and further processed using a custom script in R with the RStudio interface (R Core Team, 2019; RStudio Team, 2018). The baseline (F$_0$) of every ROI was calculated as 1% of the entire fluorescence trace per fish. Subsequently, the fractional change in fluorescence (ΔF/F$_0$) of each ROI was computed to normalize the values obtained. In order to compare basal activity between eaat2a$^{-/-}$, eaat2a$^{+/-}$ and eaat2a$^{+/+}$ larvae, the SD of F$_0$ for the whole brain was calculated and averaged over five two-minute time windows per animal (same random windows for all fish, adjusted if during seizure). Two eaat2a$^{-/-}$ larvae were excluded from SD calculations because they did not show sufficient recovery between seizures and suffered fatal seizures towards the end of recordings. Seizure duration in eaat2a$^{-/-}$ mutants was defined as the period from first time point where ΔF/F$_0$ is greater than 50% (seizure initiation) until first time point where ΔF/F$_0$ is below 50% in the midbrain. Seizure events reaching all brain parts including the anterior forebrain (telencephalon) and lasting for more than 1 min were defined as global seizures. Seizure propagation across brain parts was assessed by calculating the relative time of the peak half maxima ('pracma' package for 'findpeaks' function, R) of each brain part for all generalized seizures with a minimum peak height of 100% ΔF/F$_0$.

2.9.2 | Two-photon microscope

Two-photon calcium recordings were performed on 5 dpf eaat2a mutant Tg(gfap:Gal4)nw7;Tg(UAS:GCaMP6s) zebrafish (Diaz Verdugo et al., 2019). Larvae were preselected based on morphological

phenotype, paralyzed by injecting 1 nl of α-bungarotoxin (Invitrogen BI601, 1 mg/ml) into the spinal cord, embedded in 1.5%–2% low melting point agarose (Fisher Scientific) in a recording chamber (Fluorodish, World Precision Instruments) and constantly perfused with AFW (60 mg/L marine salt in RO water) during imaging. Imaging was performed in a two-photon microscope (Thorlabs Inc and Scientifica Inc) with a 16× water immersion objective (Nikon, NA 0.8, LWD 3.0, plan). Excitation was achieved by a mode-locked Ti:Sapphire laser (MaiTai Spectra-Physics) tuned to 920 nm. Single plane recordings of 1536 x 650 pixels were obtained at an acquisition rate of 24 Hz. The plane was oriented towards the glial cells in the boundary region between the telencephalon (anterior forebrain) and the anterior thalamus (posterior forebrain). First, spontaneous calcium activity was measured for 60 min. Subsequently for a subgroup of the fish, a custom-made Arduino was used to apply two 10-second red-light stimuli (625 nm). Light was flashed after 5 and 10 min of the total duration of 15 min.

Images were aligned, cells detected and $\Delta F/F_0$ relative to the baseline calculated using the algorithm previously described (Ohki et al., 2005; Reiten et al., 2017), with adaptions as follows. Glial cells along the ventricle were semi-automatically detected and subsequently assigned manually according to their location (Diaz Verdugo et al., 2019; Jetti et al., 2014; Reiten et al., 2017). Baseline was computed within a moving window of 80 s as the 8% of activity defining noise with a Gaussian curve fit using an adapted algorithm (Fore et al., 2020; Romano et al., 2017). Resampled $\Delta F/F_0$ traces of 4 Hz were used to detect glial calcium signals. Calcium events were identified by detecting events significantly different from noise level within a 95% confidence interval (Fore et al., 2020; Romano et al., 2017). For spontaneous recordings, glial activity was quantified in the following two-minute time windows: basal/inter-ictal (between seizure activity, averaged over six time points per fish), preictal (preceding seizure onset) and ictal (during seizure). Seizure onset frames were defined as time points where the averaged $\Delta F/F_0$ of all cells reached 50. For light stimuli recordings, glial activity was compared between 1 min prior to and 1 min following light stimuli. In each period, a cell was considered active if at least one event occurred. The overall activity of active cells was calculated by the trapezoidal numerical integration method ('trapz' function, MATLAB) to get the area under the curve (AUC). The amplitude of each event was determined as its respective maximum peak.

Light stimulus assay of neuronal activity was performed on 5 dpf $eaat2a^{+/-}$ Tg(elavl3:GCaMP6s) in-cross progenies. Mutant larvae were preselected, paralyzed and embedded as described above. After the agarose solidified for 10 min, AFW was added as an immersion medium before 20 more minutes of agarose settling. The animals were acclimatized in the setup for 20 minutes before volumetric recordings of 10 planes of 1536 x 650 pixels were obtained using a Piezo element at a rate of 2.43 Hz. Excitation was achieved as described above. Baseline spontaneous calcium activity was recorded for 10 min in darkness, followed by a red-light stimulus train using a red LED (LZ1-00R105, LedEngin; 625 nm) placed in front of the animal. Five light stimuli with five-minute inter-stimulus intervals were

applied by an Arduino-device. Images were aligned as described above. Regions of interest (ROIs) were manually drawn on one single plane of maximal information. F_0 baseline was computed as 1% of the entire fluorescence trace per ROI.

2.10 | Statistical analysis

Statistical analysis was done using R software version 3.6.0 with the RStudio version 1.2.1335 interface (R Core Team, 2019; RStudio Team, 2018) or MATLAB (Mathworks, Figure 3j and k). Data sets were tested for normality using quantile-quantile plots and Shapiro–Wilk test. Normally distributed data was analyzed using Welch two-sample unpaired t-test (Figure 5i and m). Two-sided Wilcoxon rank-sum test with continuity correction was used for nonpaired analysis (Figure 2g, Figure 3j and k, Figure 5g, h, j–l), Wilcoxon signed rank test for paired analysis (Figure 5e and f) and two-sample Kolmogorov–Smirnov test for equality between distributions (Figure 3f). Dunn Kruskal-Wallis multiple comparison test (p-adjustment: Benjamini-Hochberg method, 'FSA' package) was used for nonpaired analysis between all three genotypes (Figure 2b and c Figure 3c and Figure 4j). $p < .05$ was considered as statistically significant. Data were plotted using the 'ggplot2' package of R or MATLAB (Mathworks). Final figures were assembled using Affinity Designer Version 1.7.

2.11 | Data and code availability

The datasets and codes supporting this study have not been deposited in a public repository, but are available from the corresponding authors upon request.

3 | RESULTS

3.1 | EAAT2a is predominantly expressed in astroglial cells

To investigate the expression pattern of *eaat2a* transcripts in the larval zebrafish, we first performed in situ hybridization experiments. Our results showed that *eaat2a* transcripts are expressed in all parts of the CNS (Figure 1a). Specifically, we observed *eaat2a* transcripts along the spinal cord (Figure 1a), the periventricular zones of the forebrain, the midbrain, and the hindbrain (Figure 1b–d). In adult fish, the high expression in the forebrain (Figure 1e) and tectal periventricular regions was maintained (Figure 1f). These results suggest that spatial distribution of zebrafish *eaat2a* transcripts mainly overlaps with the location of astroglial cells, the functional homologues of mammalian astrocytes (Jurisch-Yaksi et al., 2020; Mu et al., 2019). To further confirm the precise expression of *eaat2a*, we performed triple staining using antibodies against astroglia and neuron specific proteins together with our custom made paralogue-specific antibody against EAAT2a
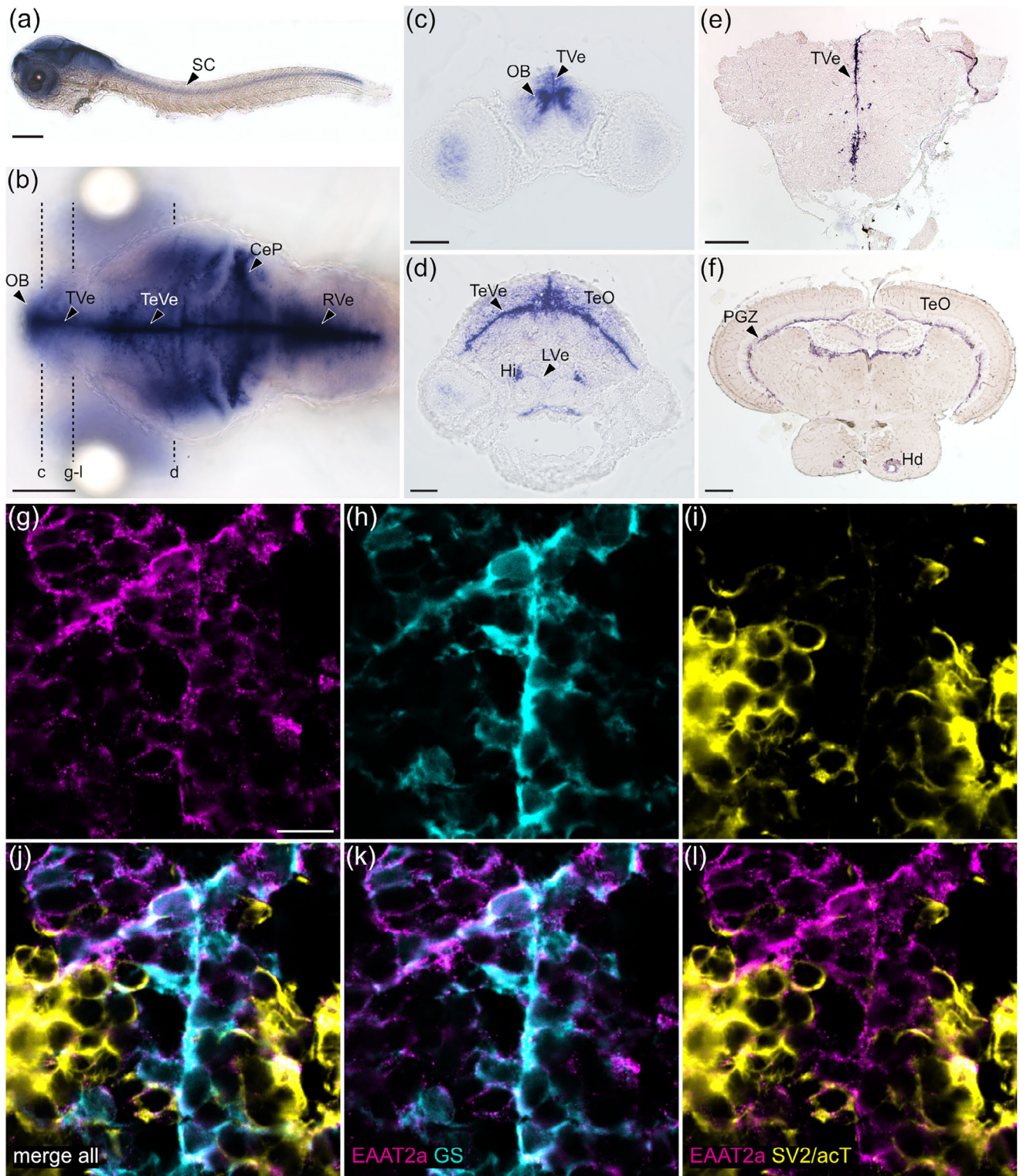
FIGURE 1 EAAT2a is predominantly expressed in astroglial cells. (a, b) mRNA of *eaat2a* was expressed along the periventricular zones (TVe, TeVe, RVe), resembling astroglial localization patterns in larval zebrafish as visible in lateral (a, 3 dpf) and dorsal (b, 5 dpf) view. (c, d) Cross sections of (b) indicated by dashed lines. (e, f) *eaat2a* mRNA expression along periventricular zones (TVe, PGZ) was maintained in adult zebrafish anterior forebrain (e) and midbrain (f). (g–i) Protein expression of EAAT2a (magenta), glutamine synthetase (GS, cyan) and synaptic vesicle 2/acetylated tubulin (SV2/acT, yellow) on cross sections of larval anterior forebrain indicated in (b). (j–l) Overlay of EAAT2a, GS and SV2/acT showed a greater co-localization of EAAT2a with astroglial (k) than neuronal (l) cells. CeP, cerebellar plate; Hi, intermediate hypothalamus; Hd, dorsal zone of periventricular hypothalamus; LVe, lateral ventricular recess of hypothalamus; OB, olfactory bulb nuclei; PGZ, periventricular gray zone of the optic tectum; TVe, periventricular zone of the telencephalon; TeO, optic tectum; TeVe, periventricular zone of the tectum; RVe, periventricular zone of the rhombencephalon. Scale bars are 200 μm in (a), (b), (e) and (f); 50 μm in (c) and (d); 10 μm in (g)
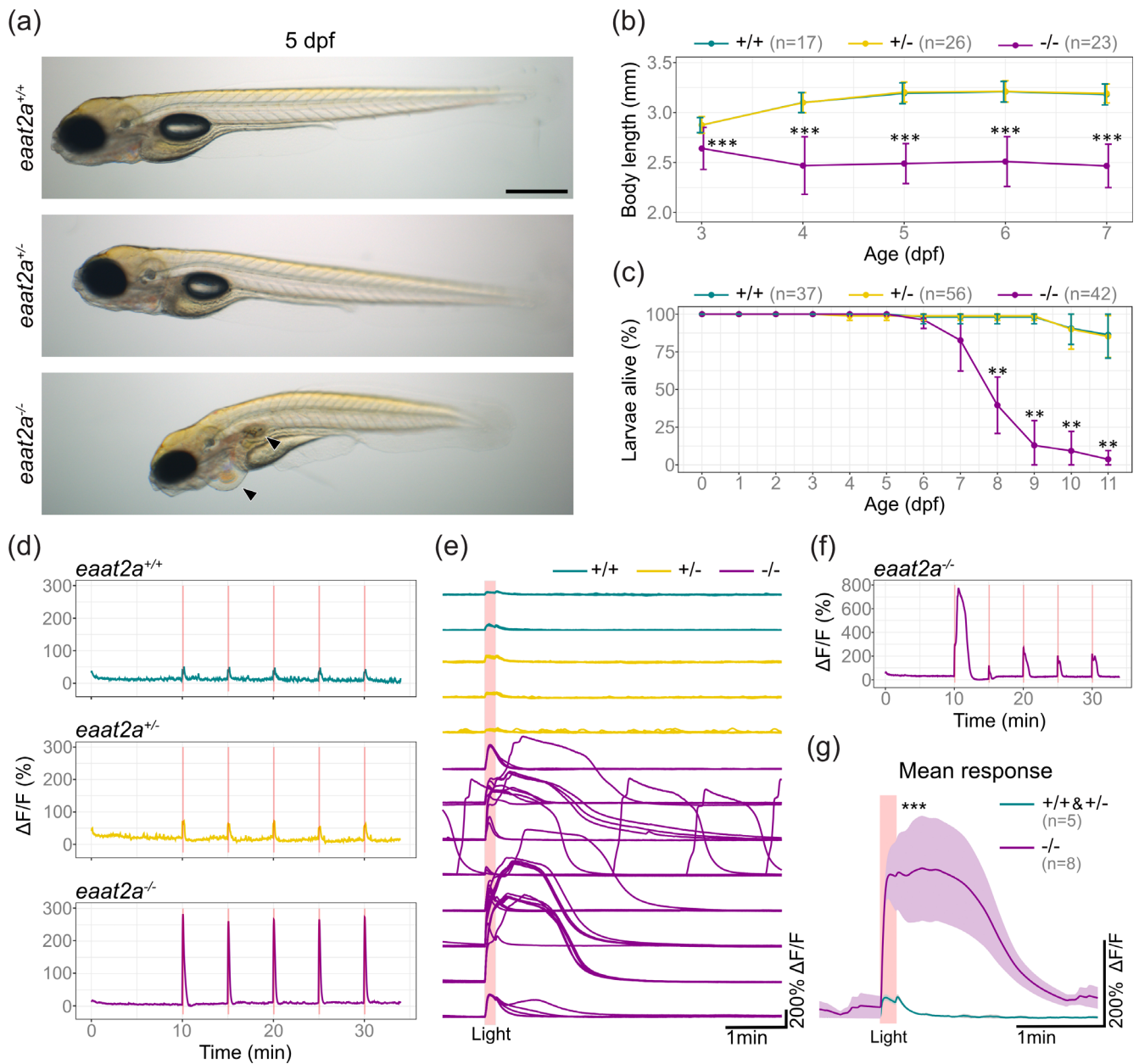
FIGURE 2 Knockout of *eaat2a* leads to hyperexcitability in response to light stimulation, morphological defects and larval lethality. (a) Lateral view of 5 dpf *eaat2a* mutants. *eaat2a*$^{-/-}$ larvae (bottom) are slightly curved, do not have an inflated swim bladder and develop pericardial edema (arrowheads). *eaat2a*$^{+/+}$ (top) and *eaat2a*$^{+/-}$ (middle) larvae are indistinguishable. Scale bar is 500 μm. (b) Spinal cord length analysis of *eaat2a* mutants at consecutive days reveals a smaller body size in *eaat2a*$^{-/-}$ (magenta) compared to their *eaat2a*$^{+/-}$ (yellow) and *eaat2a*$^{+/+}$ (cyan) siblings. Error bars show SD. (c) Mean survival of *eaat2a* mutants. Error bars show SD. (d) Whole-brain neuronal activity (*elavl3:GCaMP6s* signal) of three representative *eaat2a* mutant larvae (*eaat2a*$^{+/+}$ in cyan, *eaat2a*$^{+/-}$ in yellow and *eaat2a*$^{-/-}$ in magenta) exposed to five 10-second light stimuli with 5-minute interstimulus interval. (e) Changes in fluorescence over time ($\Delta F/F_0$) per larvae aligned at the onset of light stimuli (red line). (f) $\Delta F/F_0$ trace of an example *eaat2a*$^{-/-}$ larva with diverse responses to light-stimuli. (g) Mean responses to five light stimuli per fish in 5 dpf *eaat2a*$^{+/+}$ and *eaat2a*$^{+/-}$ (cyan, $n = 5$), and *eaat2a*$^{-/-}$ (magenta, $n = 8$) zebrafish larvae. Shaded area represents SEM. Significance level: ***$p < .001$, **$p < .01$, Dunn Kruskal Wallis multiple comparison test (b, c) or Wilcoxon rank-sum test (g). All statistics in Supplementary Table 3

(Niklaus et al., 2017) (Figure 1g–l). We found substantial co-localization of EAAT2a staining with the astroglial glutamine synthetase (GS) along the ventricular zones (Figure 1k), while neuronal cell labeling with SV2 (presynapse) and acetylated tubulin (axons) only showed weak EAAT2a signals (Figure 1l). These results demonstrate that EAAT2a is mainly expressed in astroglial cells.

3.2 | Loss of EAAT2a leads to morphological defects and larval lethality

To elucidate the function of EAAT2a in brain development and function, we generated CRISPR/Cas9-mediated knockout mutants targeting exon 3 preceding the transmembrane domains involved in
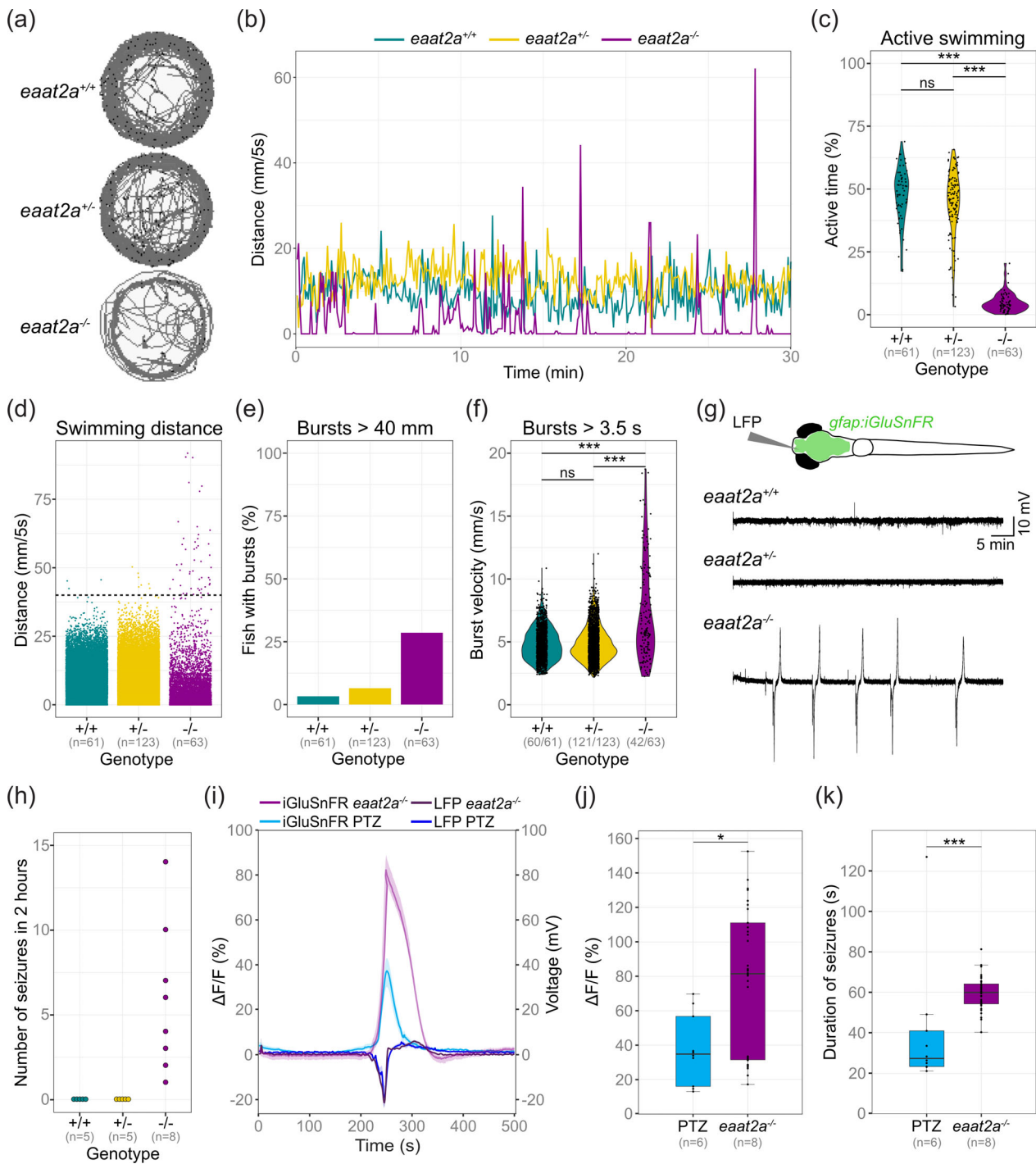
FIGURE 3 $eaat2a^{-/-}$ mutants show spontaneous seizures coinciding with a surge of extracellular glutamate. (a, b) Representative traces for swim location (a) and distances (b) over 30 min in 5 dpf $eaat2a^{-/-}$ (magenta), $eaat2a^{+/-}$ (yellow) and $eaat2a^{+/+}$ (cyan) larvae. (c) Ratio of time period with active swimming compared between $eaat2a^{-/-}$ mutants (mean 4.7%) and their $eaat2a^{+/-}$ (mean 44.4%) and $eaat2a^{+/+}$ (mean 47.6%) siblings. (d) Distance moved per five-second integral during 30-minute recordings, per genotype. Black dotted line represents threshold >40 mm/5 s. (e) Proportion of fish showing one or more bursts bigger than 40 mm during five-second integrals. (f) Velocity of all bursts lasting longer than 3.5 s compared between $eaat2a^{-/-}$ mutants (mean 7.31 mm/s) and their $eaat2a^{+/-}$ (mean 4.86 mm/s) and $eaat2a^{+/+}$ (mean 4.83) siblings. (g) Schematic illustration of simultaneous local field potential (LFP) recording and epifluorescent iGluSnFR imaging in a $Tg(gfap:iGluSnFR)$ larva (top) and representative telencephalic LFP signals. (h) Number of spontaneous global seizures detected during two-hour LFP recordings. (i) Average change in iGluSnFR fluorescence ($\Delta F/F_0$ of $gfap:iGluSnFR$ signal) and simultaneous LFP recordings during epileptic activity in 5 dpf $eaat2a^{-/-}$ mutants (shades of magenta) and PTZ-exposed wild-types (shades of blue). Signals are aligned at the onset of seizure-like events. (j) Mean amplitude of seizure-like events in PTZ-exposed (blue) and $eaat2a^{-/-}$ mutant (magenta) larvae. (k) Median duration of seizure-like events in PTZ-exposed (blue) and $eaat2a^{-/-}$ mutant (magenta) larvae. (i–k) n_{PTZ} = 6 fish, 10 seizures; $n_{eaat2a-/-}$ = 8 fish, 40 seizures. Significance levels: ***p < .001, ns = not significant (p > .05), Dunn Kruskal-Wallis multiple comparison test (c) or two-sample Kolmogorov–Smirnov test (f). All statistics in Supplementary Table 3
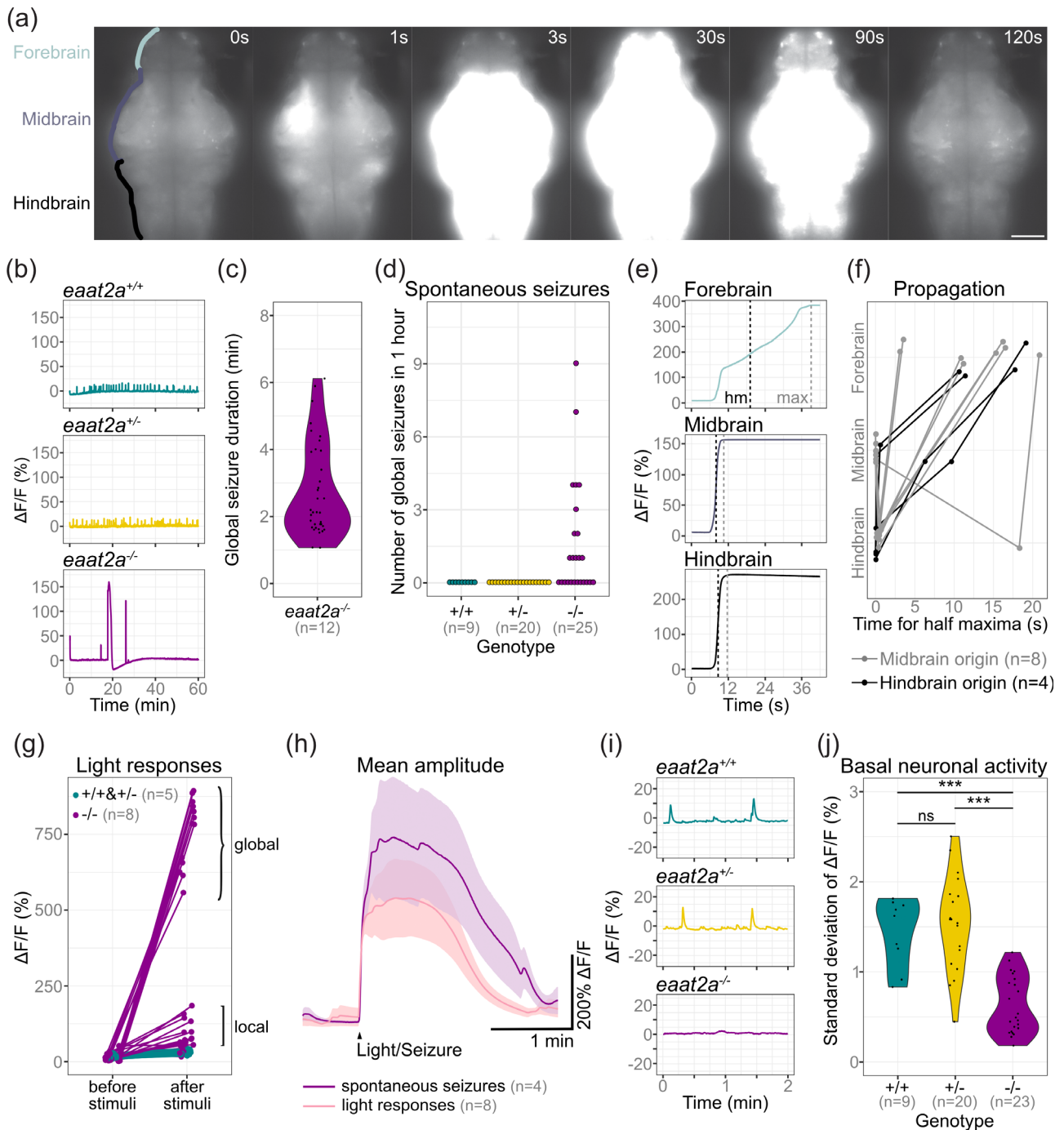
FIGURE 4 Neuronal hyperactivity during seizures contrasts with basal hypoactivity in *eaat2a*$^{-/-}$ larvae. (a) Time lapse of neuronal calcium signals during a seizure in a *eaat2a*$^{-/-}$ larva in *Tg(elavl3:GCaMP5G)* background (dorsal view). Scale bar is 100 μm. (b) Representative calcium signals (*elavl3:GCaMP5G*) recorded across the brain of *eaat2a*$^{+/+}$ (cyan, top), *eaat2a*$^{+/-}$ (yellow, middle) and *eaat2a*$^{-/-}$ (magenta, bottom) larvae. (c) Duration of spontaneous global seizures present in 12 out of 25 *eaat2a*$^{-/-}$ mutants (median 2 min 7 s [std ± 52 sec]). $n = 36$ seizures. (d) Number of spontaneous global seizures per animal recorded by calcium imaging during 60 min. (e) Neuronal activity (*elavl3:GCaMP5G*) of the three main brain regions of a representative global seizure. The half maxima (hm) represents the time point of max($\Delta F/F_0$)/2. (f) Relative time for $\Delta F/F_0$ half maximum represents propagation of global seizures across brain parts over time. Each line represents the mean relative time of one *eaat2a*$^{-/-}$ larva. Colors indicate region of seizure origin: light gray for midbrain, black for hindbrain. (g) Calcium signals (*elavl3:GCaMP6s*) 1 min before and immediately after light stimuli. Brackets indicate global (curly brackets) and local (square brackets) reflex seizures. Five light stimuli per fish. (h) Averaged calcium signals for spontaneous seizures (magenta, seven events) and light responses (light pink, 40 events) during light-stimuli recordings. Shaded area represents SEM. (i) Magnification of (b) shows calcium signals (*elavl3:GCaMP5G*) during two-minute basal activity period used for SD calculations in (j). (j) Neuronal basal activity calculated by the SD of $\Delta F/F_0$ over 2 min in *eaat2a*$^{-/-}$ mutants (mean 0.63) compared to their *eaat2a*$^{+/-}$ (mean 1.54,) and *eaat2a*$^{+/+}$ (mean 1.44,) siblings. Significance levels: ***$p < .001$, ns = not significant ($p > .05$), Dunn Kruskal-Wallis multiple comparison test. All statistics in Supplementary Table 3
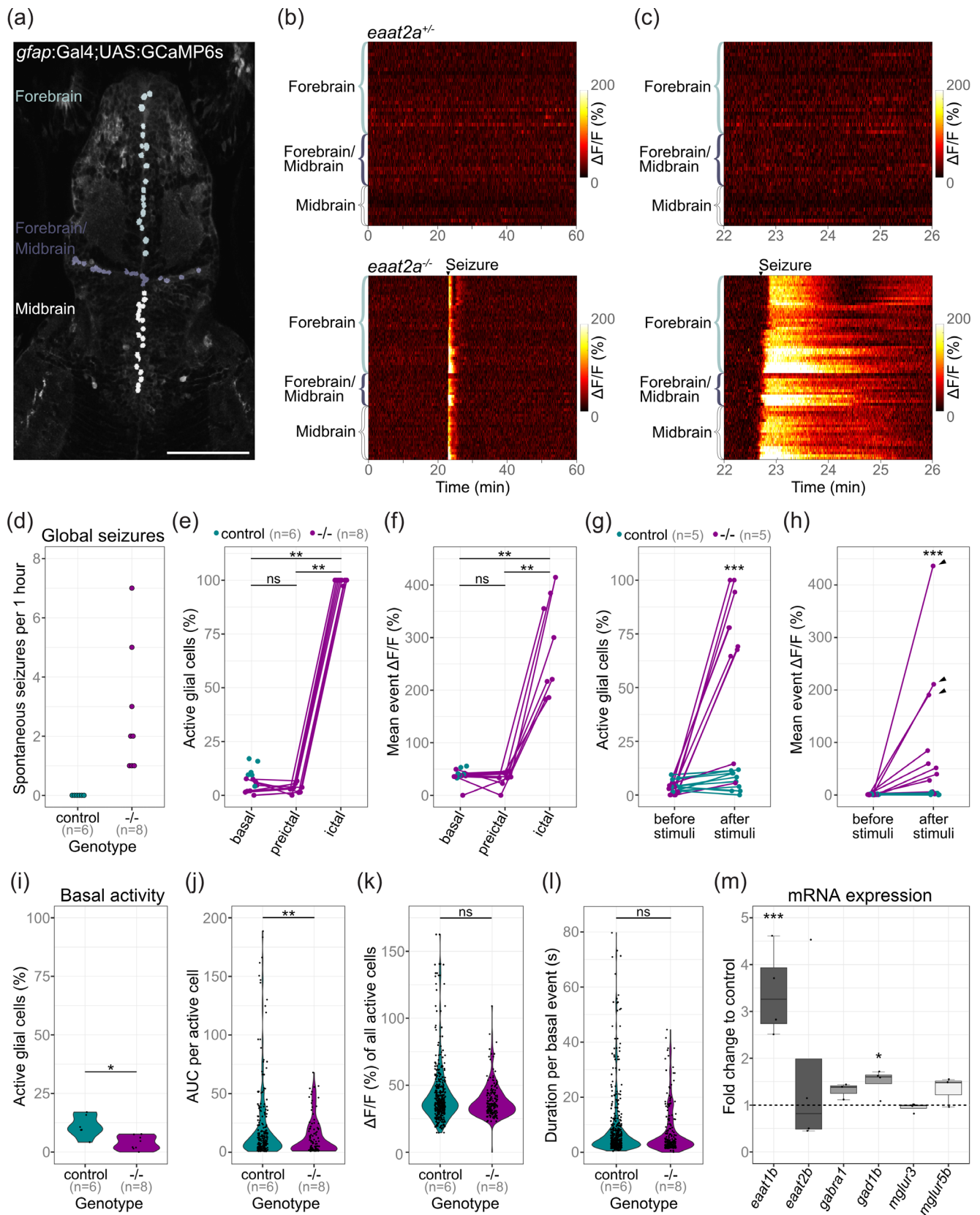
transport function (Vandenberg & Ryan, 2013a). The selected mutant allele harbors a − 13 base pair deletion, leading to premature STOP codons within the third transmembrane domain (Supplementary Figure 1). The predicted truncated protein fragment is devoid of functional transport domains, consequently no EAAT2a antibody signal was present in $eaat2a^{-/-}$ mutants (Supplementary Figure 1 and 2). We observed that $eaat2a^{-/-}$ zebrafish larvae displayed an aberrant morphology. They failed to inflate their swim bladder, developed pericardial edemas and were smaller than their siblings (Figure 2a). Body size measurements confirmed that $eaat2a^{-/-}$ zebrafish were significantly smaller than control animals at 3, 4, 5, 6, and 7 days post fertilization (dpf) (Figure 2b), with reduced brain size at 5 dpf and a transient increase in apoptotic brain cells at 4 dpf (Supplementary Figure 3). Furthermore, $eaat2a^{-/-}$ mutants were not viable past larval stage and started to die from 6 dpf on (Figure 2c). Only 10% of $eaat2a^{-/-}$ larvae were still alive at 9 dpf, and remaining survivors were heavily impaired, displaying large edemas and reduced locomotion. In contrast, $eaat2a^{+/-}$ heterozygotes were indistinguishable from $eaat2a^{+/+}$ siblings by visual inspection.

3.3 | $eaat2a^{-/-}$ mutant zebrafish exhibit hyperexcitability in response to light stimulation

EAAT2 is an essential part of the glutamate clearance mechanism in the brain (Danbolt, 2001; Niklaus et al., 2017). Hence, the absence of the glutamate transporter may lead to changes in neuronal excitability in $eaat2a^{-/-}$ mutant zebrafish. To test this hypothesis, we compared brain-wide neuronal responses to transient light flashes in $eaat2a^{-/-}$ zebrafish and control siblings expressing the transgenic calcium indicator GCaMP6s under the neuronal elavl3 promoter (Diaz Verdugo et al., 2019). We observed that $eaat2a^{-/-}$ mutant larvae displayed highly amplified light responses compared to their $eaat2a^{+/-}$ and $eaat2a^{+/+}$ siblings (Figure 2d and e), with varying response amplitudes across and within $eaat2a^{-/-}$ larvae (Figure 2f). Strikingly, average neuronal responses in $eaat2a^{-/-}$ larvae were not only excessively

enlarged, but also very long lasting (Figure 2g). Occasionally, we also observed spontaneous neuronal activity bursts of similar magnitude (Figure 2e), potentially resembling spontaneous epileptic seizures (Fisher et al., 2014; Gawel, Langlois et al., 2020; Hortopan et al., 2010; Yaksi et al., 2021). Taken together, our results show that $eaat2a^{-/-}$ zebrafish brains exhibit increased excitability in responses to light stimulation and are possibly prone to epileptic seizures.

3.4 | $eaat2a^{-/-}$ mutant zebrafish show spontaneous seizures coinciding with a surge of extracellular glutamate

Our neuronal activity recordings suggested that $eaat2a^{-/-}$ mutant zebrafish not only exhibit strong light-induced responses but also display occasional neuronal activity bursts resembling epileptic seizures. To further characterize this spontaneous seizure-like phenotype in $eaat2a^{-/-}$ mutants, we examined swimming behavior in 5 dpf larvae by using automated behavioral tracking. We observed that $eaat2a^{+/+}$ and $eaat2a^{+/-}$ zebrafish swim with periods of stop, slow and fast swims as described previously in healthy zebrafish (Budick & O'Malley, 2000; Kalueff et al., 2013). In contrast, $eaat2a^{-/-}$ mutant animals displayed aberrant locomotor patterns (Figure 3a–f). $eaat2a^{-/-}$ larvae swam substantially less than their $eaat2a^{+/-}$ and $eaat2a^{+/+}$ siblings, mainly lying motionless on the bottom of the dish (Figure 3a–c). Strikingly, when $eaat2a^{-/-}$ larvae swam, they showed convulsive twitching and swim bursts occasionally followed by swirling around their body axis and finally immobilized sinking to the bottom of the dish (Supplementary Movie 1). Compared to their siblings, $eaat2a^{-/-}$ zebrafish showed more swim bursts of either long distance (Figure 3d and e) or high velocity during a prolonged period (Figure 3f, Supplementary Figure 4). This swirling and bursting behavior highly resembles established models of epilepsy and is interpreted as seizure-like behavior in zebrafish (Baraban et al., 2005; Hortopan et al., 2010). All these findings support the idea that $eaat2a^{-/-}$ larvae exhibit spontaneous seizures.

FIGURE 5 Astroglial network in $eaat2a^{-/-}$ mutants is silent yet hyperexcitable. (a) Two-photon microscopy image of the forebrain and midbrain in a 5 dpf Tg(gfap:Gal4;UAS:GCaMP6s) zebrafish larva expressing GCaMP6s in GFAP positive glial cells. Individual astroglia along the ventricular regions are color-coded according to three different areas: forebrain (light gray), forebrain/midbrain boundary region (dark gray), and midbrain (white). Scale bar is 100 μm. (b) Calcium signals ($\Delta F/F_0$) of individual glial cells over time in representative $eaat2a^{+/-}$ (top) and $eaat2a^{-/-}$ (bottom) larvae. Warm color indicates high activity as seen during the seizure in the $eaat2a^{-/-}$ larva. (c) Four-minute periods of calcium signals in (b). (d) Number of global seizures detected in $eaat2a^{-/-}$ mutants (magenta) compared to their $eaat2a^{+/-}$ and $eaat2a^{+/+}$ siblings (cyan). (e, f) Percentage of active glial cells (e) and average event amplitudes of active cells (f) of individual $eaat2a^{-/-}$ mutants during two-minute basal/inter-ictal, preictal and ictal (spontaneous seizures) periods. Cyan dots show average basal values of $eaat2a^{+/+}$ and $eaat2a^{+/-}$ siblings. Figure legend in (e) also applies to (f). (g, h) Evaluation of one-minute periods immediately before and after 10-second light stimuli in $eaat2a^{+/+}/eaat2a^{+/-}$ (cyan) and $eaat2a^{-/-}$ (magenta) animals of the proportion of active cells (g) and averaged amplitude over all cells (h). Arrowheads indicate global seizures. $n = 5$ fish per group, 2 stimuli per fish. Figure legend in (g) also applies to (h). (i–l) Analysis during inter-ictal basal periods of percentage active astroglia per fish (i), total activity of active cells (j, area under the curve = AUC), amplitudes (k) and durations (l) of individual calcium bursts in active glial cells are plotted in violin plots with individual data points (black). Control = $eaat2a^{+/+}$ and $eaat2a^{+/-}$. (m) mRNA transcript levels of eaat1b, eaat2b, gabra1, gad1b, mglur3 and mglur5b in 5 dpf $eaat2a^{-/-}$ relative to $eaat2a^{+/+}$ siblings. Transcripts were measured by RT-qPCR and normalized to g6pd and b2m. Data are represented in box-and-whisker plots with an interquartile range from first to third quartile and the median represented by the line within the boxes. Significance levels: ***$p < .001$, **$p < .01$, *$p < .05$, ns = not significant ($p > .05$), Wilcoxon signed rank test (e, f), Welch two sample unpaired t-test (i, m) or Wilcoxon rank-sum test (g, h, j–l). All statistics in Supplementary Table 3

To verify the presence of seizure-activity in $eaat2a^{-/-}$ mutant brains, we measured local field potentials (LFPs) by inserting a microelectrode in the anterior forebrain (telencephalon) of 5 dpf animals. As expected, the measured electrical activity in $eaat2a^{-/-}$ larvae revealed spontaneous episodes of high voltage LFP deflections (Figure 3g). These signals resembled seizure-like LFP activity in other zebrafish models, where seizures were pharmacologically induced by pentylenetetrazole (PTZ), a γ-aminobutyric acid (GABA) A receptor antagonist (Diaz Verdugo et al., 2019; Liu & Baraban, 2019; Turrini et al., 2017). Such spontaneous seizures were not detected in $eaat2a^{+/-}$ or $eaat2a^{+/+}$ siblings (Figure 3g and h). We hypothesized that spontaneous seizures in $eaat2a^{-/-}$ mutant larvae are associated with an excess of extracellular glutamate that cannot be removed due to impaired astroglial glutamate clearance (Hanson et al., 2019). Hence, we expected that glutamate surges during spontaneous seizures would occur to a greater extent than in PTZ-induced seizures in animals with intact glutamate clearance (Diaz Verdugo et al., 2019). To test this hypothesis, we combined LFP measurements with simultaneous fluorescence recordings of extracellular glutamate near astroglial terminals using $Tg(gfap:iGluSnFR)$ animals (MacDonald et al., 2016). In $eaat2a^{-/-}$ larvae, we observed massive increases of iGluSnFR signals reflecting glutamate levels, coinciding with spontaneous electrographic seizures (Figure 3i). These iGluSnFR signals in $eaat2a^{-/-}$ larvae had higher amplitudes (Figure 3j) and lasted longer (Figure 3k) as compared to PTZ-induced seizures, although the LFP deflections were comparable (Figure 3i). Taken together, our results suggest that loss of EAAT2a causes a slowed glutamate clearance, leading to excessive extracellular glutamate levels, and thereby lowering the threshold for epileptic seizures.

3.5 | Neuronal hyperactivity during seizures contrasts with basal hypoactivity in $eaat2a^{-/-}$ larvae

To characterize EAAT2a-related seizures further, we investigated neuronal activity in 5 dpf $Tg(elavl3:GCaMP5G)$ zebrafish. Our recordings revealed recurrent periods of excessive neuronal activity spreading across the entire brain of $eaat2a^{-/-}$ mutants (Figure 4a, Supplementary Movies 2 and 3). During these spontaneous seizures, neuronal calcium signals across the brain reached levels greater than 100% of relative change in fluorescence (ΔF/F) (Figure 4b bottom). These globally high levels of neuronal seizure-activity were maintained for more than a minute before decreasing to a short hypoactive period, and finally returning to inter-ictal (between seizures) levels (Figure 4b bottom and 4c). These results confirm that $eaat2a^{-/-}$ mutants exhibit spontaneous global seizures that are not present in $eaat2a^{+/-}$ and $eaat2a^{+/+}$ control siblings (Figure 4d). In addition to these global seizures, we found that some larvae additionally or exclusively showed localized seizures not reaching the anterior forebrain and lasting for less than a minute (Supplementary Figure 5).

Next, we asked how different brain regions are recruited during seizure propagation in $eaat2a^{-/-}$ mutants. As represented in Figure 4e, excessive increase in intracellular calcium levels was initiated in the midbrain (8 of 12 fish) or hindbrain (4 of 12 fish). To quantify this further, we compared half maxima of neuronal calcium signals (ΔF/F₀) between anterior forebrain, midbrain and hindbrain during global seizures lasting for more than 1 min. We observed that neurons of the anterior forebrain were recruited only seconds after seizure initiation (mean 13 s, SD ± 5.67 s), regardless of the seizure origin (Figure 4f). Beyond these spontaneous seizures, we also observed that the large amplitude light responses shown earlier in Figure 2e were very similar to spontaneous global (Figure 4g, curly brackets) and localized (Figure 4g, square brackets) seizures with comparable amplitudes (Figure 4h). Since epileptic seizures that are objectively and consistently evoked by a specific external stimulus are referred to as reflex seizures, we termed these excessive responses to light in $eaat2a^{-/-}$ mutants as light-induced reflex seizures (Koepp et al., 2016).

Intriguingly, during inter-ictal periods, $eaat2a^{-/-}$ mutants exhibited reduced basal neuronal activity compared to $eaat2a^{+/-}$ and $eaat2a^{+/+}$ siblings (Figure 4i). We observed smaller fluctuations (SD) of neuronal calcium signals in $eaat2a^{-/-}$ larvae compared to their siblings (Figure 4j). This reduced basal activity might explain hypoactive locomotor behaviors of $eaat2a^{-/-}$ mutants (Figure 3c). Taken together, our results indicate that loss of EAAT2a not only leads to spontaneous seizures, but also reduces basal neuronal activity during inter-ictal periods. Moreover, in all our experiments, $eaat2a^{+/-}$ mutants were indistinguishable from their $eaat2a^{+/+}$ siblings, suggesting that $eaat2a^{+/-}$ mutation does not lead to haploinsufficiency or any seizure phenotype.

3.6 | Astroglial network in $eaat2a^{-/-}$ mutants is silent yet hyperexcitable

Given the predominant astroglial expression of EAAT2a, one potential cause for the reduced neuronal basal activity in $eaat2a^{-/-}$ mutants may be the impaired astroglial glutamate recycling, which reduces available glutamate. To investigate whether astroglial function is impaired in $eaat2a^{-/-}$ mutants, we recorded glial calcium signals in 5 dpf larvae expressing GCaMP6s under the glial promoter $gfap$ ($Tg(gfap:Gal4)nw7;Tg(UAS:GCaMP6s)$) (Diaz Verdugo et al., 2019). To exclusively analyze astroglial activity, we focused on the region along the ventricular zones in the forebrain and midbrain (Figure 5a). In line with our previous results, we observed spontaneous events of excessive astroglial activity (ΔF/F₀ greater than 100%) spreading across the entire brain of $eaat2a^{-/-}$ mutants (Figure 5b), often finally recruiting the anterior forebrain (Figure 5c, Supplementary Movies 4 and 5). These events likely represent astroglial activity during seizures (Diaz Verdugo et al., 2019). Such spontaneous global events were prominent at least once per hour in $eaat2a^{-/-}$ mutants and absent in $eaat2a^{+/-}$ and $eaat2a^{+/+}$ control siblings (Figure 5d). To further characterize astroglial activity, we quantified the ratio of active glial cells and the amplitudes per calcium burst in $eaat2a^{-/-}$ mutant larvae during basal/inter-ictal, preictal (preceding seizure onset) and ictal periods. We observed a drastic increase in the ratio of active astroglia and amplitude of calcium bursts at the transition from preictal to ictal
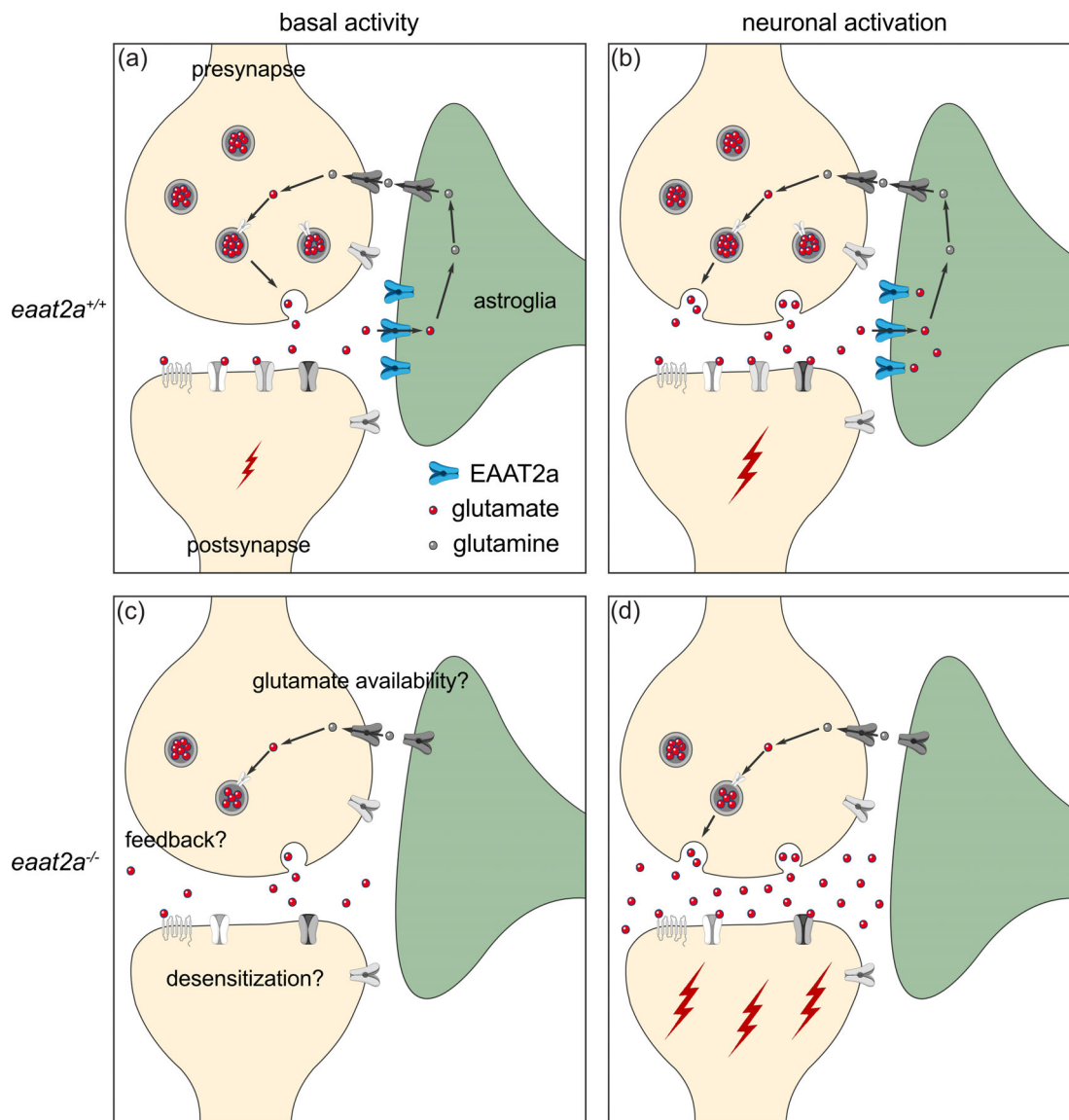
FIGURE 6 Working model of coexisting hyper- and hypoactivity in $eaat2a^{-/-}$ mutants. (a, b) Glutamate transporter EAAT2a is important for both clearance of glutamate at the synaptic cleft and recycling of glutamate to the presynapse during basal activity (a) and neuronal activation (b). (c) Loss of EAAT2a function leads to neuronal hypoactivity during basal periods, potentially reflecting reduced levels of available glutamate/glutamine. (d) Once glutamate is released in higher quantities from the presynapse (e.g., following light stimuli or spontaneous glutamate release), astroglia cannot sufficiently take up glutamate. Accumulated glutamate in the synaptic cleft hyperexcites postsynaptic neurons, which can lead to a cascade of glutamate release across the nervous system and results in epileptic seizures. Such recurrent epileptic seizures could also potentially lead to desensitization or a negative feedback to the presynapse (c), which can further explain reduced basal neuronal activity in $eaat2a^{-/-}$ mutants

period, while inter-ictal and preictal periods appeared to be similar (Figure 5e and f). Next, we tested whether these large bursts of astroglial calcium signals are also present in light-evoked seizures. Our results revealed that the ratio and the amplitude of astroglial calcium signals were significantly larger in $eaat2a^{-/-}$ mutants, when compared to control siblings (Figure 5g and h). Furthermore, some of these light-evoked seizures propagated globally, recruiting the entire brain including the anterior forebrain (Figure 5h, arrowheads). During inter-ictal periods, a smaller ratio of astroglial cells were active (Figure 5i), and these active cells had reduced overall activity (Figure 5j) in $eaat2a^{-/-}$

mutants compared to their siblings. However, we did not observe a significant difference in the amplitude or the duration of individual astroglial calcium bursts between $eaat2a^{-/-}$ mutants and control siblings during inter-ictal/basal periods (Figure 5k and l). Taken together, our results reveal that astroglial cells in $eaat2a^{-/-}$ mutants are less active during inter-ictal states, and generate excessive calcium bursts only during seizures.

The depressed yet hyperexcitable brain state of $eaat2a^{-/-}$ mutants implies pathological changes in the brain. To test the impact of $eaat2a$ loss on the gene expression of key regulators of neuronal

and astroglial activity, we analyzed whole-brain transcript levels using quantitative reverse transcription PCR (RT-qPCR). Firstly, we tested for transcriptional adaptation of other *eaat* glutamate transporters. Expression levels of *eaat2b*, the *eaat2a* paralogue, did not differ in *eaat2a*$^{-/-}$ animals (Figure 5m). In contrast, another glutamate transporter *eaat1b* was upregulated in *eaat2a*$^{-/-}$ mutants compared to *eaat2a*$^{+/+}$ siblings (Figure 5m), suggesting a compensatory effect to improve buffering of excess synaptic glutamate in *eaat2a*$^{-/-}$ mutants (Figure 3i). Second, we assessed whether expressions of genes associated with inhibitory neurotransmission of GABA are altered. We found that the expression of the GABA$_A$ receptor subunit *gabra1* did not differ between *eaat2a*$^{-/-}$ and *eaat2a*$^{+/+}$ brains (Figure 5m). There was an increase in the presynaptic enzyme *gad1b* in *eaat2a*$^{-/-}$ mutants ($p = 0.024$), yet given the considerable variance and a mean fold change of 1.5, the biological relevance remains unclear. Finally, we investigated whether metabotropic glutamate receptors (mGluRs) on astroglia are affected. These receptors can influence intracellular calcium transients in astroglia following synaptic glutamate release (Bazargani & Attwell, 2016). In *eaat2a*$^{-/-}$ larval brains, we observed no difference in expression levels of glial expressed *mglur3* or brain abundant (Haug et al., 2013) *mglur5b*. This suggests that reduced inter-ictal activity in *eaat2a*$^{-/-}$ mutant astroglia is not due to impaired mGluR-induced calcium signaling. Taken together, the altered gene expression levels of *eaat1b* in *eaat2a*$^{-/-}$ mutants suggest a compensatory attempt to adjust increased brain excitability by buffering glutamate.

4 | DISCUSSION

We show that glutamate transporter EAAT2a is required to balance brain excitability by regulating extracellular glutamate levels. Our results indicate that impaired EAAT2a function results in epileptic seizures but also reduced basal brain activity (Figure 6).

Epileptic seizures are due to an imbalance between excitatory and inhibitory synaptic transmission. In this study, we show that a genetic perturbation of the excitatory glutamate system leads to profound functional alterations in neuronal and astroglial networks, leading to spontaneous and light-induced seizures. Our results are in line with the earlier observations associating EAAT2 malfunctions to seizures in mice and humans (Epi4K Consortium et al., 2013; Epi4K Consortium, 2016; Guella et al., 2017; Petr et al., 2015; Stergachis et al., 2019; Tanaka et al., 1997; Wagner et al., 2018). In addition, our novel *eaat2a*$^{-/-}$ mutant zebrafish epilepsy model has several important characteristics. Firstly, homozygous mutations of the astroglial *eaat2a* in zebrafish resemble a form of DEE present in human epilepsy patients with de novo mutations in the orthologous gene (EAAT2 = SLC1A2) (Epi4K Consortium et al., 2013; Epi4K Consortium, 2016; Guella et al., 2017). DEE is clinically defined as a condition where developmental defects due to a mutation as well as epileptic activity itself contribute to the impairments (Scheffer et al., 2017). The presence of both recurrent spontaneous seizures and severe developmental abnormalities in *eaat2a*$^{-/-}$ mutants mirror the human

phenotype (Epi4K Consortium, 2016; Guella et al., 2017). Second, spontaneous recurrent seizures in our *eaat2a*$^{-/-}$ mutants enable the investigation of epileptogenesis throughout development. Although *eaat2a*$^{-/-}$ mutants' premature death restricts analysis to larval stages, future work on an inducible gene knockout would allow studies at more advanced developmental stages (Niklaus & Neuhauss, 2017). Finally, knockout of EAAT2a directly targets mainly astroglial networks, which are of great importance during seizure initiation and propagation (Devinsky et al., 2013; Diaz Verdugo et al., 2019; Steinhäuser et al., 2012). Therefore, our model will enable further investigations into the role of glia–neuron interactions in epilepsy. All these points give a novel vantage point for modeling and understanding potential mechanisms underlying human genetic epilepsies.

Recent studies show that astroglia and their interactions with neurons play an essential role in epilepsy (Devinsky et al., 2013; Diaz Verdugo et al., 2019; Seifert & Steinhäuser, 2013; Steinhäuser et al., 2012). The role of astroglial gap junctions in redistributing ions and neurotransmitters in epilepsy models are well investigated (Boison & Steinhäuser, 2018; Steinhäuser et al., 2012). However, the function of astroglial glutamate transporters in epilepsy are less understood. Our results provide direct evidence for the importance of astroglial glutamate transporters for balancing brain excitability. On the one hand, in the absence of glutamate transporter EAAT2a, which is predominantly expressed on astroglia, we observed spontaneous seizures recruiting both neuronal and astroglial networks. In addition, light-induced reflex seizures are apparent in both cellular networks. Such evidence of hyperexcitability is likely due to impaired glutamate clearance in *eaat2a*$^{-/-}$ mutants, leading to a massive transient surge of extracellular glutamate (Hanson et al., 2019), as measured by iGluSnFR imaging. The observed upregulation of glutamate transporter *eaat1b* transcripts further supports this hypothesis. On the other hand, we observed that both neuronal and astroglial networks are hypoactive during inter-ictal periods. We argue that this hypoactive state might reflect the reduced availability of glutamate due to depletion of the presynaptic glutamate pool after seizures in combination with impaired glutamate recycling. Since astroglial uptake of glutamate is impaired in *eaat2a*$^{-/-}$ mutants, the conversion of glutamate to glutamine is likely reduced, resulting in an impaired glutamate-glutamine cycle (Bak et al., 2006). This eventually leads to lesser glutamate reconversion in the presynaptic neurons, leading to hypoactivity (Tani et al., 2014). Alternatively, impaired glutamate clearance from the synaptic cleft can lead to desensitization or reduction of postsynaptic glutamate receptors, especially ionotropic AMPA receptors (Jayakar & Dikshit, 2004; Trussell & Fischbach, 1989). Consequently, the sensitivity to basal extracellular glutamate fluctuations may be decreased in these animals, and only higher levels of extracellular glutamate induced by sensory stimulation lead to the observed hyperexcitability. A third possibility is that the spontaneous release of glutamate from the presynapse may be suppressed by a negative feedback by neuropeptide modulators. As such, neuropeptide Y, which indirectly inhibits presynaptic glutamate release, has been shown to be upregulated in patients with resistant epilepsy and rodent models (Furtinger et al., 2001; Tu et al., 2005). It is likely that

all these mechanisms contribute to the switch between the hypoactive inter-ictal state and epileptic seizures. In fact, not only the recurrent spontaneous seizures of eaat2a⁻/⁻ mutants, but also the reduced inter-ictal brain activity mirror observations in human patients; de novo mutations in the human orthologue EAAT2 cause profound intellectual disability (Epi4K Consortium, 2016; Guella et al., 2017).

In recent years, pharmacological and genetic zebrafish models have been used to advance the understanding of epileptogenesis (Afrikanova et al., 2013; Baraban et al., 2005; Diaz Verdugo et al., 2019; Gawel, Turski et al., 2020; Ghannad-Rezaie et al., 2019; Ibhazehiebo et al., 2018; Liao et al., 2019; Liu & Baraban, 2019; Samarut et al., 2018; Sourbron et al., 2019; Tiraboschi et al., 2020; Turrini et al., 2017; Yaksi et al., 2021). Many of these studies focus on the inhibitory system by either pharmacologically or genetically manipulating GABA receptors. However, a better understanding of the major excitatory neurotransmitter system is of great importance, also considering that glutamate is the primary precursor of GABA (Bak et al., 2006). In our model of targeting the glutamate transporter EAAT2a, we found several similarities to existing zebrafish models. Considering seizure propagation, we found that seizures in eaat2a⁻/⁻ mutants initiate in midbrain and hindbrain regions that include important primary processing areas such as the optic tectum (homologous to mammalian superior colliculus [Mueller, 2012]) and the cerebellum (Kita et al., 2015). Interestingly, the anterior forebrain (homologous to mammalian neocortex [Ito & Yamamoto, 2009]) is recruited only with a significant delay. Compared to the PTZ-induced model leading to a lack of neuronal inhibition, our results are similar to findings of one study (Diaz Verdugo et al., 2019), yet contradicting another study showing epileptic propagation from anterior to posterior brain regions (Liu & Baraban, 2019). However, both studies found neuronal microcircuits to be a crucial step in seizure propagation. In line with this idea, we observed not only global but also localized seizures in eaat2a⁻/⁻ mutants, all starting in subcortical regions. These findings support the hypothesis that highly connected hub-like regions play an important role as gate keepers between seizure foci and global brain networks (Paz & Huguenard, 2015). Furthermore, it suggests that the recruitment of seizure-prone (ictogenic) hubs during seizure propagation might be more crucial than the initial dysfunction itself. It is likely that this recruitment of specific circuits is dependent on the current brain state, which has been suggested to influence seizure probability (Staba & Worrell, 2014). In fact, eaat2a⁻/⁻ animals suffering global reflex seizures also always exhibited spontaneous global seizures. Hence, future studies in our model may help to understand the transition from local to global seizure networks, and the role of astroglia in these transitions.

We also observed fundamental differences between our eaat2a⁻/⁻ mutants and existing zebrafish models. Our model reflects that epilepsy is more than just a seizure disorder. In fact, subsequent neurobiological and cognitive consequences are part of the epilepsy definition (Fisher et al., 2014). While existing zebrafish models helped to observe several aspects of epileptic hyperexcitability (Diaz Verdugo et al., 2019; Liu & Baraban, 2019; Samarut et al., 2018; Turrini et al., 2017; Yaksi et al., 2021), our eaat2a⁻/⁻ mutants display reduced inter-ictal brain activity. The low neuronal and astroglial network activity in eaat2a⁻/⁻ mutants likely is associated with pathological changes in the brain (Scheffer et al., 2017), potentially corresponding to intellectual disabilities in patients with EAAT2 de novo mutations (Epi4K Consortium, 2016; Guella et al., 2017). We also observed decreased brain size in eaat2a⁻/⁻ larvae, possibly reflecting cerebral atrophy found in patients with EAAT2 mutations (Epi4K Consortium, 2016; Guella et al., 2017). Furthermore, our findings on overall reduced locomotion in eaat2a⁻/⁻ zebrafish is consistent with reduced muscle tone in human patients (Epi4K Consortium, 2016; Guella et al., 2017). Hence, relying solely on increased locomotion as seizure readout in zebrafish models may miss important aspects of epilepsy (Yaksi et al., 2021). Accordingly, focusing not only on the seizure-related hyperactivity but also on the pathophysiology of reduced inter-ictal activity might help unraveling important underlying details of the combined clinical presentation of DEE.

Our findings in eaat2a⁻/⁻ mutant zebrafish may also have a broader relevance for epilepsy research. The current clinical dichotomy between focal and generalized seizures is operational and may not reflect mechanistic distinctions (Fernandez-Baca Vaca & Park, 2020; Fisher et al., 2017; Wolf & Beniczky, 2014). Recent research in human patients using advanced neurophysiological methods and functional imaging is transforming our understanding on ictogenesis. Even the archetypical 'generalized' absence seizures involve rather selective parts of the brain, and not the entire cortex as suggested by conventional scalp electroencephalogram (Bai et al., 2010; Wolf & Beniczky, 2014). Our transparent zebrafish model enables detailed whole-brain imaging of widespread glia–neuron networks (Ahrens et al., 2012; Wyatt et al., 2015). We observed at high temporal resolution a local subcortical seizure origin and subsequent global propagation. It has been proposed that all seizures in fact initiate within local networks, and subsequent spreading results from a lost balance between local and global network connectivity (Blumenfeld, 2014; Stam, 2016). Subcortical networks are likely of particular interest, given that they have been shown to be intimately involved in seizures traditionally thought to arise from cortical lobes (Motelow et al., 2015; Picard et al., 2006). Furthermore, the eaat2a⁻/⁻ model enables a certain temporal control of seizure onset through light-induction, providing a prominent window to study ictogenesis. Future studies in our eaat2a⁻/⁻ model may help to improve the understanding on interactions between local and global seizure networks. For all these reasons, we propose to use our novel epilepsy model comprehensively to further the understanding of underlying epileptogenic mechanisms. Given the ease of pharmacological manipulation of the zebrafish, we argue that our astroglial eaat2a⁻/⁻ mutant model will provide an unexplored platform for identifying new treatment approaches, especially taking into account glial mechanisms as a promising novel target (Cunliffe et al., 2015; Eimon et al., 2018; Riquelme et al., 2020; Sourbron et al., 2019; Yaksi et al., 2021; Zhang et al., 2015).

CONFLICT OF INTEREST

The authors declare no competing interests.

AUTHOR CONTRIBUTIONS

Adriana L. Hotz, Nathalie Jurisch-Yaksi, Emre Yaksi and Stephan C.F. Neuhauss conceptualized the study; Adriana L. Hotz, Ahmed Jamali, Nicolas N. Rieser, Stephanie Niklaus and Ecem Aydin performed experiments; Adriana L. Hotz, Ahmed Jamali, Nicolas N. Rieser, Ecem Aydin, Nathalie Jurisch-Yaksi and Emre Yaksi analyzed data; Adriana L. Hotz, Ahmed Jamali, Laetitia Lalla, Nathalie Jurisch-Yaksi and Emre Yaksi developed custom R and MATLAB codes; Adriana L. Hotz, Ahmed Jamali, Nathalie Jurisch-Yaksi and Emre Yaksi prepared all figures; Adriana L. Hotz, Nathalie Jurisch-Yaksi, Emre Yaksi and Stephan C.F. Neuhauss wrote the manuscript; Adriana L. Hotz, Ahmed Jamali, Sverre Myren-Svelstad, Nathalie Jurisch-Yaksi, Emre Yaksi and Stephan C.F. Neuhauss edited the manuscript with the help of all authors; Nathalie Jurisch-Yaksi, Emre Yaksi and Stephan C.F. Neuhauss acquired funding and supervised the students.

DATA AVAILABILITY STATEMENT

The datasets and codes supporting this study have not been deposited in a public repository, but are available from the corresponding authors upon request.

ORCID

Adriana L. Hotz https://orcid.org/0000-0003-1992-7829
Nicolas N. Rieser https://orcid.org/0000-0001-5902-1269
Stephanie Niklaus https://orcid.org/0000-0002-8045-2335
Sverre Myren-Svelstad https://orcid.org/0000-0003-4258-8028
Nathalie Jurisch-Yaksi https://orcid.org/0000-0002-8767-6120
Emre Yaksi https://orcid.org/0000-0003-3761-0235
Stephan C. F. Neuhauss https://orcid.org/0000-0002-9615-480X

REFERENCES

Afrikanova, T., Serruys, A.-S. K., Buenafe, O. E. M., Clinckers, R., Smolders, I., de Witte, P. A. M., Crawford, A. D., & Esguerra, C. V. (2013). Validation of the zebrafish pentylenetetrazol seizure model: Locomotor versus electrographic responses to antiepileptic drugs. *PLoS One*, 8(1), e54166. https://doi.org/10.1371/journal.pone.0054166

Ahrens, M. B., Li, J. M., Orger, M. B., Robson, D. N., Schier, A. F., Engert, F., & Portugues, R. (2012). Brain-wide neuronal dynamics during motor adaptation in zebrafish. *Nature*, 485(7399), 471–477. https://doi.org/10.1038/nature11057

Akerboom, J., Chen, T.-W., Wardill, T. J., Tian, L., Marvin, J. S., Mutlu, S., Calderon, N. C., Esposti, F., Borghuis, B. G., Sun, X. R., Gordus, A., Orger, M. B., Portugues, R., Engert, F., Macklin, J. J., Filosa, A., Aggarwal, A., Kerr, R. A., Takagi, R., ... Looger, L. L. (2012). Optimization of a GCaMP calcium indicator for neural activity imaging. *The Journal Of Neuroscience: The Official Journal Of The Society For Neuroscience*, 32(40), 13819–13840. https://doi.org/10.1523/JNEUROSCI.2601-12.2012

Allen, N. J., & Eroglu, C. (2017). Cell biology of astrocyte-synapse interactions. *Neuron*, 96(3), 697–708. https://doi.org/10.1016/j.neuron.2017.09.056

Bai, X., Vestal, M., Berman, R., Negishi, M., Spann, M., Vega, C., Desalvo, M., Novotny, E. J., Constable, R. T., & Blumenfeld, H. (2010). Dynamic time course of typical childhood absence seizures: Eeg, behavior, and functional magnetic resonance imaging. *The Journal Of Neuroscience: The Official Journal Of The Society For Neuroscience*, 30(17), 5884–5893. https://doi.org/10.1523/JNEUROSCI.5101-09.2010

Bak, L. K., Schousboe, A., & Waagepetersen, H. S. (2006). The glutamate/GABA-glutamine cycle: Aspects of transport, neurotransmitter homeostasis and ammonia transfer. *Journal of Neurochemistry*, 98(3), 641–653. https://doi.org/10.1111/j.1471-4159.2006.03913.x

Baraban, S. C., Taylor, M. R., Castro, P. A., & Baier, H. (2005). Pentylenetetrazole induced changes in zebrafish behavior, neural activity and c-fos expression. *Neuroscience*, 131(3), 759–768. https://doi.org/10.1016/j.neuroscience.2004.11.031

Bazargani, N., & Attwell, D. (2016). Astrocyte calcium signaling: The third wave. *Nature Neuroscience*, 19(2), 182–189. https://doi.org/10.1038/nn.4201

Blumenfeld, H. (2014). What is a seizure network? Long-range network consequences of focal seizures. *Advances in Experimental Medicine and Biology*, 813, 63–70. https://doi.org/10.1007/978-94-017-8914-1_5

Boison, D., & Steinhäuser, C. (2018). Epilepsy and astrocyte energy metabolism. *Glia*, 66(6), 1235–1243. https://doi.org/10.1002/glia.23247

Budick, S. A., & O'Malley, D. M. (2000). Locomotor repertoire of the larval zebrafish: Swimming, turning and prey capture. *The Journal of Experimental Biology*, 203(Pt 17), 2565–2579.

Clarke, L. E., & Barres, B. A. (2013). Emerging roles of astrocytes in neural circuit development. *Nature Reviews. Neuroscience*, 14(5), 311–321. https://doi.org/10.1038/nrn3484

Coulter, D. A., & Eid, T. (2012). Astrocytic regulation of glutamate homeostasis in epilepsy. *Glia*, 60(8), 1215–1226. https://doi.org/10.1002/glia.22341

Coulter, D. A., & Steinhäuser, C. (2015). Role of astrocytes in epilepsy. *Cold Spring Harbor Perspectives in Medicine*, 5(3), a022434–a022434. https://doi.org/10.1101/cshperspect.a022434

Cunliffe, V. T., Baines, R. A., Giachello, C. N. G., Lin, W.-H., Morgan, A., Reuber, M., Russell, C., Walker, M. C., & Williams, R. S. B. (2015). Epilepsy research methods update: Understanding the causes of epileptic seizures and identifying new treatments using non-mammalian model

organisms. *Seizure*, 24, 44–51. https://doi.org/10.1016/j.seizure.2014.09.018

Danbolt, N. C. (2001). Glutamate uptake. *Progress in Neurobiology*, 65(1), 1–105.

Devinsky, O., Vezzani, A., Najjar, S., de Lanerolle, N. C., & Rogawski, M. A. (2013). Glia and epilepsy: Excitability and inflammation. *Trends in Neurosciences*, 36(3), 174–184. https://doi.org/10.1016/j.tins.2012.11.008

Diaz Verdugo, C., Myren-Svelstad, S., Aydin, E., van Hoeymissen, E., Deneubourg, C., Vanderhaeghe, S., Vancraeynest, J., Pelgrims, R., Cosacak, M. I., Muto, A., Kizil, C., Kawakami, K., Jurisch-Yaksi, N., & Yaksi, E. (2019). Glia-neuron interactions underlie state transitions to generalized seizures. *Nature Communications*, 10(1), 475. https://doi.org/10.1038/s41467-019-11739-z

Eid, T., Lee, T.-S. W., Patrylo, P., & Zaveri, H. P. (2019). Astrocytes and glutamine Synthetase in Epileptogenesis. *Journal of Neuroscience Research*, 97(11), 1345–1362. https://doi.org/10.1002/jnr.24267

Eimon, P. M., Ghannad-Rezaie, M., de Rienzo, G., Allalou, A., Wu, Y., Gao, M., Roy, A., Skolnick, J., & Yanik, M. F. (2018). Brain activity patterns in high-throughput electrophysiology screen predict both drug efficacies and side effects. *Nature Communications*, 9(1), 219. https://doi.org/10.1038/s41467-017-02404-4

Epi4K Consortium, Epilepsy Phenome/Genome Project, Allen, A. S., Berkovic, S. F., Cossette, P., Delanty, N., Dlugos, D., Eichler, E. E., Epstein, E. P., Glauser, T., Goldstein, D. B, Han, Y., Heinzen, E. L., Hitomi, Y., Howell, K. B., Johnson, M. R., Kuzniecky, R., Lowenstein, D. H., & Winawer, M. R. (2013). De novo mutations in epileptic encephalopathies. *Nature*, 501(7466), 217–221. https://doi.org/10.1038/nature12439

Epi4K Consortium. (2016). De novo mutations in SLC1A2 and CACNA1A are important causes of epileptic encephalopathies. *American Journal of Human Genetics*, 99(2), 287–298. https://doi.org/10.1016/j.ajhg.2016.06.003

Fernandez-Baca Vaca, G., & Park, J. T. (2020). Focal EEG abnormalities and focal ictal semiology in generalized epilepsy. *Seizure*, 77, 7–14. https://doi.org/10.1016/j.seizure.2019.12.013

Fisher, R. S., Acevedo, C., Arzimanoglou, A., Bogacz, A., Cross, J. H., Elger, C. E., Engel, J., Jr., Forsgren, L., French, J. A., Glynn, M., Hesdorffer, D. C., Lee, B. I., Mathern, G. W., Moshé, S. L., Perucca, E., Scheffer, I. E., Tomson, T., Watanabe, M., & Wiebe, S. (2014). Ilae official report: A practical clinical definition of epilepsy. *Epilepsia*, 55(4), 475–482. https://doi.org/10.1111/epi.12550

Fisher, R. S., Cross, J. H., French, J. A., Higurashi, N., Hirsch, E., Jansen, F. E., Lagae, L., Moshé, S. L., Peltola, J., Roulet Perez, E., Scheffer, I. E., & Zuberi, S. M. (2017). Operational classification of seizure types by the international league against epilepsy: Position paper of the ILAE Commission for Classification and Terminology. *Epilepsia*, 58(4), 522–530. https://doi.org/10.1111/epi.13670

Fore, S., Acuña-Hinrichsen, F., Mutlu, K. A., Bartoszek, E. M., Serneels, B., Faturos, N. G., Chau, K. T. P., Cosacak, M. I., Verdugo, C. D., Palumbo, F., Ringers, C., Jurisch-Yaksi, N., Kizil, C., & Yaksi, E. (2020). Functional properties of habenular neurons are determined by developmental stage and sequential neurogenesis. *Science Advances*, 6(36), eaaz3173. https://doi.org/10.1126/sciadv.aaz3173

Furtinger, S., Pirker, S., Czech, T., Baumgartner, C., Ransmayr, G., & Sperk, G. (2001). Plasticity of Y1 and Y2 receptors and neuropeptide Y fibers in patients with temporal lobe epilepsy. *The Journal Of Neuroscience: The Official Journal Of The Society For Neuroscience*, 21(15), 5804–5812.

Gagnon, J. A., Valen, E., Thyme, S. B., Huang, P., Akhmetova, L., Pauli, A., Montague, T. G., Zimmerman, S., Richter, C., & Schier, A. F. (2014). Efficient mutagenesis by Cas9 protein-mediated oligonucleotide insertion and large-scale assessment of single-guide RNAs. *PLoS One*, 9(5), e98186. https://doi.org/10.1371/journal.pone.0098186

Gawel, K., Langlois, M., Martins, T., van der Ent, W., Tiraboschi, E., Jacmin, M., Crawford, A. D., & Esguerra, C. V. (2020). Seizing the

moment: Zebrafish epilepsy models. *Neuroscience and Biobehavioral Reviews*, 116, 1–20. https://doi.org/10.1016/j.neubiorev.2020.06.010

Gawel, K., Turski, W. A., van der Ent, W., Mathai, B. J., Kirstein-Smardzewska, K. J., Simonsen, A., & Esguerra, C. V. (2020). Phenotypic characterization of larval zebrafish (Danio rerio) with partial knockdown of the cacna1a gene. *Molecular Neurobiology*, 57(4), 1904–1916. https://doi.org/10.1007/s12035-019-01860-x

Gesemann, M., Lesslauer, A., Maurer, C. M., Schonthaler, H. B., & Neuhauss, S. C. F. (2010). Phylogenetic analysis of the vertebrate excitatory/neutral amino acid transporter (SLC1/EAAT) family reveals lineage specific subfamilies. *BMC Evolutionary Biology*, 10, 117. https://doi.org/10.1186/1471-2148-10-117

Ghannad-Rezaie, M., Eimon, P. M., Wu, Y., & Yanik, M. F. (2019). Engineering brain activity patterns by neuromodulator polytherapy for treatment of disorders. *Nature Communications*, 10(1), 2620. https://doi.org/10.1038/s41467-019-10541-1

Guella, I., McKenzie, M. B., Evans, D. M., Buerki, S. E., Toyota, E. B., van Allen, M. I., Epilepsy Genomics Study, Suri, M., Elmslie, F., Deciphering Developmental Disorders Study, Simon, M. E. H., van Gassen, K. L. I., Héron, D., Keren, B., Nava, C., Connolly, M. B., Demos, M., & Farrer, M. J. (2017). De novo mutations in YWHAG cause early-onset epilepsy. *American Journal of Human Genetics*, 101(2), 300–310. https://doi.org/10.1016/j.ajhg.2017.07.004

Hanson, E., Armbruster, M., Lau, L. A., Sommer, M. E., Klaft, Z.-J., Swanger, S. A., Traynelis, S. F., Moss, S. J., Noubary, F., Chadchankar, J., & Dulla, C. G. (2019). Tonic activation of GluN2C/GluN2D-containing NMDA receptors by ambient glutamate facilitates cortical interneuron maturation. *The Journal Of Neuroscience: The Official Journal Of The Society For Neuroscience*, 39(19), 3611–3626. https://doi.org/10.1523/JNEUROSCI.1392-18.2019

Haug, M. F., Gesemann, M., Mueller, T., & Neuhauss, S. C. F. (2013). Phylogeny and expression divergence of metabotropic glutamate receptor genes in the brain of zebrafish (Danio rerio). *The Journal of Comparative Neurology*, 521(7), 1533–1560. https://doi.org/10.1002/cne.23240

Hortopan, G. A., Dinday, M. T., & Baraban, S. C. (2010). Zebrafish as a model for studying genetic aspects of epilepsy. *Disease Models & Mechanisms*, 3(3–4), 144–148. https://doi.org/10.1242/dmm.002139

Huang, Y. Y., Haug, M. F., Gesemann, M., & Neuhauss, S. C. F. (2012). Novel expression patterns of metabotropic glutamate receptor 6 in the zebrafish nervous system. *PLoS ONE* 7(4), e35256. https://doi.org/10.5167/uzh-63265

Ibhazehiebo, K., Gavrilovici, C., De La Hoz, C. L., de Ma, S.-C., Rehak, R., Kaushik, G., Meza Santoscoy, P. L., Scott, L., Nath, N., Kim., D.-Y., Rho, J. M., & Kurrasch, D. M. (2018). A novel metabolism-based phenotypic drug discovery platform in zebrafish uncovers HDACs 1 and 3 as a potential combined anti-seizure drug target. *Brain: A Journal of Neurology*, 141(3), 744–761. https://doi.org/10.1093/brain/awx364

Isogai, S., Horiguchi, M., & Weinstein, B. M. (2001). The vascular anatomy of the developing zebrafish: An atlas of embryonic and early larval development. *Developmental Biology*, 230(2), 278–301. https://doi.org/10.1006/dbio.2000.9995

Ito, H., & Yamamoto, N. (2009). Non-laminar cerebral cortex in teleost fishes? *Biology Letters*, 5(1), 117–121. https://doi.org/10.1098/rsbl.2008.0397

Jayakar, S. S., & Dikshit, M. (2004). Ampa receptor regulation mechanisms: Future target for safer neuroprotective drugs. *The International Journal of Neuroscience*, 114(6), 695–734. https://doi.org/10.1080/00207450490430453

Jetti, S. K., Vendrell-Llopis, N., & Yaksi, E. (2014). Spontaneous activity governs olfactory representations in spatially organized habenular microcircuits. *Current Biology: CB*, 24(4), 434–439. https://doi.org/10.1016/j.cub.2014.01.015

Jurisch-Yaksi, N., Yaksi, E., & Kizil, C. (2020). Radial glia in the zebrafish brain: Functional, structural, and physiological comparison with the

mammalian glia. *Glia. Advance online publication.*, *68*, 2451–2470. https://doi.org/10.1002/glia.23849

Kalueff, A. V., Gebhardt, M., Stewart, A. M., Cachat, J. M., Brimmer, M., Chawla, J. S., … Schneider, H. (2013). Towards a comprehensive catalog of zebrafish behavior 1.0 and beyond. *Zebrafish*, *10*(1), 70–86. https://doi.org/10.1089/zeb.2012.0861

Kita, E. M., Scott, E. K., & Goodhill, G. J. (2015). Topographic wiring of the retinotectal connection in zebrafish. *Developmental Neurobiology*, *75*(6), 542–556. https://doi.org/10.1002/dneu.22256

Koepp, M. J., Caciagli, L., Pressler, R. M., Lehnertz, K., & Beniczky, S. (2016). Reflex seizures, traits, and epilepsies: From physiology to pathology. *The Lancet Neurology*, *15*(1), 92–105. https://doi.org/10.1016/S1474-4422

Lambert, C. J., Freshner, B. C., Chung, A., Stevenson, T. J., Bowles, D. M., Samuel, R., Gale, B. K., & Bonkowsky, J. L. (2018). An automated system for rapid cellular extraction from live zebrafish embryos and larvae: Development and application to genotyping. *PLoS One*, *13*(3), e0193180. https://doi.org/10.1371/journal.pone.0193180

Liao, M., Kundap, U., Rosch, R. E., Burrows, D. R. W., Meyer, M. P., Bencheikh, B. O. A., Cossette, P., & Samarut, É. (2019). Targeted knockout of GABA receptor gamma 2 subunit provokes transient light-induced reflex seizures in zebrafish larvae. *Disease Models & Mechanisms. Advance online publication.* *12*(11), dmm040782. https://doi.org/10.1242/dmm.040782

Liu, J., & Baraban, S. C. (2019). Network properties revealed during multiscale calcium imaging of seizure activity in zebrafish. *ENeuro*, *6*(1), ENEURO.0041, ENEU19.2019. https://doi.org/10.1523/ENEURO.0041-19.2019

MacDonald, R. B., Kashikar, N. D., Lagnado, L., & Harris, W. A. (2016). A novel tool to measure extracellular glutamate in the zebrafish nervous system in vivo. *Zebrafish. Advance online publication.*, *14*, 284–286. https://doi.org/10.1089/zeb.2016.1385

Mathieson, W. B., & Maler, L. (1988). Morphological and electrophysiological properties of a novel in vitro preparation: The electrosensory lateral line lobe brain slice. *Journal of Comparative Physiology. A, Sensory, Neural, and Behavioral Physiology*, *163*(4), 489–506. https://doi.org/10.1007/BF00604903

Motelow, J. E., Li, W., Zhan, Q., Mishra, A. M., Sachdev, R. N. S., Liu, G., Gummadavelli, A., Zayyad, Z., Lee, H. S., Chu, V., Andrews, J. P., Englot, D. J., Herman, P., Sanganahalli, B. G., Hyder, F., & Blumenfeld, H. (2015). Decreased subcortical cholinergic arousal in focal seizures. *Neuron*, *85*(3), 561–572. https://doi.org/10.1016/j.neuron.2014.12.058

Mu, Y., Bennett, D. V., Rubinov, M., Narayan, S., Yang, C.-T., Tanimoto, M., Mensh, B. D., Looger, L. L., & Ahrens, M. B. (2019). Glia accumulate evidence that actions are futile and suppress unsuccessful behavior. *Cell*, *178*(1), 27–43.e19. https://doi.org/10.1016/j.cell.2019.05.050

Mueller, T. (2012). What is the thalamus in zebrafish? *Frontiers in Neuroscience*, *6*, 64. https://doi.org/10.3389/fnins.2012.00064

Mullins, M. C., Hammerschmidt, M., Haffter, P., & Nusslein-Volhard, C. (1994). Large-scale mutagenesis in the zebrafish: In search of genes controlling development in a vertebrate. *Current Biology: CB*, *4*(3), 189–202.

Muto, A., Lal, P., Ailani, D., Abe, G., Itoh, M., & Kawakami, K. (2017). Activation of the hypothalamic feeding Centre upon visual prey detection. *Nature Communications*, *8*, 15029. https://doi.org/10.1038/ncomms15029

Niklaus, S., Cadetti, L., Vom Berg-Maurer, C. M., Lehnherr, A., Hotz, A. L., Forster, I. C., Gesemann, M., & Neuhauss, S. C. F. (2017). Shaping of signal transmission at the photoreceptor synapse by EAAT2 glutamate transporters. *ENeuro*, *4*(3), ENEU16.2017. ENEURO.0339-16.2017. https://doi.org/10.1523/ENEURO.0339-16.2017

Niklaus, S., & Neuhauss, S. C. F. (2017). Genetic approaches to retinal research in zebrafish. *Journal of Neurogenetics*, *31*, 1–18. https://doi.org/10.1080/01677063.2017.1343316

Ohki, K., Chung, S., Ch'ng, Y. H., Kara, P., & Reid, R. C. (2005). Functional imaging with cellular resolution reveals precise micro-architecture in visual cortex. *Nature*, *433*(7026), 597–603. https://doi.org/10.1038/nature03274

Paz, J. T., & Huguenard, J. R. (2015). Microcircuits and their interactions in epilepsy: Is the focus out of focus? *Nature Neuroscience*, *18*(3), 351–359. https://doi.org/10.1038/nn.3950

Petr, G. T., Sun, Y., Frederick, N. M., Zhou, Y., Dhamne, S. C., Hameed, M. Q., Miranda, C., Bedoya, E. A., Fischer, K. D., Armsen, W., Wang, J., Danbolt, N. C., Rotenberg, A., Aoki, C. J., & Rosenberg, P. A. (2015). Conditional deletion of the glutamate transporter GLT-1 reveals that astrocytic GLT-1 protects against fatal epilepsy while neuronal GLT-1 contributes significantly to glutamate uptake into synaptosomes. *The Journal Of Neuroscience: The Official Journal Of The Society For Neuroscience*, *35*(13), 5187–5201. https://doi.org/10.1523/JNEUROSCI.4255-14.2015

Picard, F., Bruel, D., Servent, D., Saba, W., Fruchart-Gaillard, C., Schöllhorn-Peyronneau, M.-A., Roumenov, D., Brodtkorb, E., Zuberi, S., Gambardella, A., Steinborn, B., Hufnagel, A., Valette, H., & Bottlaender, M. (2006). Alteration of the in vivo nicotinic receptor density in ADNFLE patients: A PET study. *Brain: A Journal of Neurology*, *129*(Pt 8), 2047–2060. https://doi.org/10.1093/brain/awl156

R: A Language and Environment for Statistical Computing (Version 3.6.0) [Computer software] (2019). R Foundation for Statistical Computing. Vienna, Austria: R Foundation for Statistical Computing. https://www.R-project.org/

Reiten, I., Uslu, F. E., Fore, S., Pelgrims, R., Ringers, C., Diaz Verdugo, C., Hoffman, M., Lal, P., Kawakami, K., Pekkan, K., Yaksi, E., & Jurisch-Yaksi, N. (2017). Motile-cilia-mediated flow improves sensitivity and temporal resolution of olfactory computations. *Current Biology: CB*, *27*(2), 166–174. https://doi.org/10.1016/j.cub.2016.11.036

Riquelme, J., Wellmann, M., Sotomayor-Zárate, R., & Bonansco, C. (2020). Gliotransmission: A novel target for the development of Antiseizure drugs. *The Neuroscientist: A Review Journal Bringing Neurobiology, Neurology and Psychiatry*, *26*(4), 293–309. https://doi.org/10.1177/1073858420901474

Romano, S. A., Pérez-Schuster, V., Jouary, A., Boulanger-Weill, J., Candeo, A., Pietri, T., & Sumbre, G. (2017). An integrated calcium imaging processing toolbox for the analysis of neuronal population dynamics. *PLoS Computational Biology*, *13*(6), e1005526. https://doi.org/10.1371/journal.pcbi.1005526

Rosch, R. E., & Dulla, C. G. (2020). A tale of two networks-glial Contributions to generalized seizures. *Epilepsy Currents*, *20*(2), 108–110. https://doi.org/10.1177/1535759720906115

Rothstein, J. D., Dykes-Hoberg, M., Pardo, C. A., Bristol, L. A., Jin, L., Kuncl, R. W., Kanai, Y., Hediger, M. A., Wang, Y., Schielke, J. P., & Welty, D. F. (1996). Knockout of glutamate transporters reveals a major role for Astroglial transport in excitotoxicity and clearance of glutamate. *Neuron*, *16*(3), 675–686. https://doi.org/10.1016/S0896-6273

RStudio: Integrated Development for R (Version 1.2.1335) [Computer software] (2018). RStudio, Inc., Boston, MA: RStudio, Inc., Boston, MA. http://www.rstudio.com/

Samarut, É., Swaminathan, A., Riché, R., Liao, M., Hassan-Abdi, R., Renault, S., Allard, M., Dufour, L., Cossette, P., Soussi-Yanicostas, N., & Drapeau, P. (2018). Γ-aminobutyric acid receptor alpha 1 subunit loss of function causes genetic generalized epilepsy by impairing inhibitory network neurodevelopment. *Epilepsia*, *59*(11), 2061–2074. https://doi.org/10.1111/epi.14576

Santello, M., Toni, N., & Volterra, A. (2019). Astrocyte function from information processing to cognition and cognitive impairment. *Nature Neuroscience*, *22*(2), 154–166. https://doi.org/10.1038/s41593-018-0325-8

Scheffer, I. E., Berkovic, S., Capovilla, G., Connolly, M. B., French, J., Guilhoto, L., Hirsch, E., Jain, S., Mathern, G. W., Moshé, S. L., Nordli, D. R., Perucca, E., Tomson, T., Wiebe, S., Zhang, Y. H., & Zuberi, S. M. (2017). Ilae classification of the epilepsies: Position paper of the ILAE commission for classification and terminology. *Epilepsia*, *58*(4), 512–521. https://doi.org/10.1111/epi.13709

Schindelin, J., Arganda-Carreras, I., Frise, E., Kaynig, V., Longair, M., Pietzsch, T., Preibisch, S., Rueden, C., Saalfeld, S., Schmid, B., Tinevez, J.-Y., White, D. J., Hartenstein, V., Eliceiri, K., Tomancak, P., & Cardona, A. (2012). Fiji: an open-source platform for biological-image analysis. *Nature Methods*, *9*(7), 676–682. https://doi.org/10.1038/nmeth.2019

Seifert, G., & Steinhäuser, C. (2013). Neuron-astrocyte signaling and epilepsy. *Experimental Neurology*, *244*, 4–10. https://doi.org/10.1016/j.expneurol.2011.08.024

Sourbron, J., Partoens, M., Scheldeman, C., Zhang, Y., Lagae, L., & de Witte, P. (2019). Drug repurposing for Dravet syndrome in scn1Lab−/− mutant zebrafish. *Epilepsia*, *60*(2), e8–e13. https://doi.org/10.1111/epi.14647

Staba, R. J., & Worrell, G. A. (2014). What is the importance of abnormal "background" activity in seizure generation? *Advances in Experimental Medicine and Biology*, *813*, 43–54. https://doi.org/10.1007/978-94-017-8914-1_3

Stam, C. J. (2016). Epilepsy: What can we learn from modern network theories. *Epileptologie*, *33*, 38–43.

Steinhäuser, C., Seifert, G., & Bedner, P. (2012). Astrocyte dysfunction in temporal lobe epilepsy: K+ channels and gap junction coupling. *Glia*, *60*(8), 1192–1202. https://doi.org/10.1002/glia.22313

Stergachis, A. B., Pujol-Giménez, J., Gyimesi, G., Fuster, D., Albano, G., Troxler, M., Picker, J., Rosenberg, P. A., Bergin, A., Peters, J., el Achkar, C. M., Harini, C., Manzi, S., Rotenberg, A., Hediger, M. A., & Rodan, L. H. (2019). Recurrent SLC1A2 variants cause epilepsy via a dominant negative mechanism. *Annals of Neurology. Advance online publication*, *85*, 921–926. https://doi.org/10.1002/ana.25477

Tanaka, K., Watase, K., Manabe, T., Yamada, K., Watanabe, M., Takahashi, K., Iwama, H., Nishikawa, T., Ichihara, N., Kikuchi, T., Okuyama, S., Kawashima, N., Hori, S., Takimoto, M., & Wada, K. (1997). Epilepsy and exacerbation of brain injury in mice lacking the glutamate transporter GLT-1. *Science (New York, N.Y.)*, *276*(5319), 1699–1702. https://doi.org/10.1126/science.276.5319.1699

Tani, H., Dulla, C. G., Farzampour, Z., Taylor-Weiner, A., Huguenard, J. R., & Reimer, R. J. (2014). A local glutamate-glutamine cycle sustains synaptic excitatory transmitter release. *Neuron*, *81*(4), 888–900. https://doi.org/10.1016/j.neuron.2013.12.026

Tiraboschi, E., Martina, S., van der van der Ent, W., Grzyb, K., Gawel, K., Cordero-Maldonado, M. L., Poovathingal, S. K., Heintz, S., Satheesh, S. V., Brattespe, J., Xu, J., Suster, M., Skupin, A., & Esguerra, C. V. (2020). New insights into the early mechanisms of epileptogenesis in a zebrafish model of Dravet syndrome. *Epilepsia*, *61*(3), 549–560. https://doi.org/10.1111/epi.16456

Trussell, L. O., & Fischbach, G. D. (1989). Glutamate receptor desensitization and its role in synaptic transmission. *Neuron*, *3*(2), 209–218. https://doi.org/10.1016/0896-6273

Tu, B., Timofeeva, O., Jiao, Y., & Nadler, J. V. (2005). Spontaneous release of neuropeptide Y tonically inhibits recurrent mossy fiber synaptic transmission in epileptic brain. *The Journal Of Neuroscience: The Official Journal Of The Society For Neuroscience*, *25*(7), 1718–1729. https://doi.org/10.1523/JNEUROSCI.4835-04.2005

Turrini, L., Fornetto, C., Marchetto, G., Müllenbroich, M. C., Tiso, N., Vettori, A., Resta, F., Masi, A., Mannaioni, G., Pavone, F. S., & Vanzi, F. (2017). Optical mapping of neuronal activity during seizures in zebrafish. *Scientific Reports*, *7*(1), 3025. https://doi.org/10.1038/s41598-017-03087-z

Vandenberg, R. J., & Ryan, R. M. (2013a). Mechanisms of glutamate transport. *Physiological Reviews*, *93*(4), 1621–1657. https://doi.org/10.1152/physrev.00007.2013

Vladimirov, N., Mu, Y., Kawashima, T., Bennett, D. V., Yang, C.-T., Looger, L. L., Keller, P. J., Freeman, J., & Ahrens, M. B. (2014). Light-sheet functional imaging in fictively behaving zebrafish. *Nature Methods*, *11*(9), 883–884. https://doi.org/10.1038/nmeth.3040

Wagner, M., Gusic, M., Günthner, R., Alhaddad, B., Kovacs-Nagy, R., Makowski, C., Baumeister, F., Strom, T., Meitinger, T., Prokisch, H., & Wortmann, S. B. (2018). Biallelic mutations in SLC1A2; an additional mode of inheritance for SLC1A2-related epilepsy. *Neuropediatrics*, *49*(1), 59–62. https://doi.org/10.1055/s-0037-1606370

Wilkinson, R. N., Elworthy, S., Ingham, P. W., & van Eeden, F. J. M. (2013). A method for high-throughput PCR-based genotyping of larval zebrafish tail biopsies. *BioTechniques*, *55*(6), 314–316. https://doi.org/10.2144/000114116

Wolf, P., & Beniczky, S. (2014). Understanding ictogenesis in generalized epilepsies. *Expert Review of Neurotherapeutics*, *14*(7), 787–798. https://doi.org/10.1586/14737175.2014.925803

Wyatt, C., Bartoszek, E. M., & Yaksi, E. (2015). Methods for studying the zebrafish brain: Past, present and future. *The European Journal of Neuroscience*, *42*(2), 1746–1763. https://doi.org/10.1111/ejn.12932

Yaksi, E., Jamali, A., Diaz Verdugo, C., & Jurisch-Yaksi, N. (2021). Past, present and future of zebrafish in epilepsy research. *The FEBS Journal Advance Online Publication. (Epub ahead of print)*, https://doi.org/10.1111/febs.15694

Zhang, Y., Kecskés, A., Copmans, D., Langlois, M., Crawford, A. D., Ceulemans, B., Lagae, L., De Witte, P. A. M., & Esguerra, C. V. (2015). Pharmacological characterization of an antisense knockdown zebrafish model of Dravet syndrome: Inhibition of epileptic seizures by the serotonin agonist fenfluramine. *PLoS One*, *10*(5), e0125898. https://doi.org/10.1371/journal.pone.0125898

SUPPORTING INFORMATION

Additional supporting information may be found in the online version of the article at the publisher's website.